23 Single-Molecule Detection

Detection of single molecules represents the ultimate level of sensitivity and has been a longstanding goal of analytical methods. Because of its high sensitivity, and because a bright signal appears against a dark background, fluorescence is one obvious choice for single-molecule detection (SMD). However, SMD using fluorescence is technically difficult. The first report on SMD using fluorescence with a single fluorophore at room temperature appeared just 15 years ago in 1990.[1] In that report SMD was accomplished under flow conditions to minimize the observed volume. Pulsed laser excitation was used to allow off-gating of the scattered light, which otherwise obscured the signal. Even with careful optical filtering and solvent purification the detected signal was only about 50 photons per molecule of rhodamine 6G in water, with background counts of up to 20 photons. This work[1] demonstrated that SMD would be a difficult task, particularly in less pure biological samples. The literature contains earlier reports of SMD. These include the report by Hirshfeld in 1976[2] and reports by Keller, Mathies, and coworkers in 1989.[3–4] However, these experiments were performed with large molecules, each of which contained multiple fluorophores. In Hirshfeld's work the protein–polymer complex contained about 100 fluorescein molecules.[2] In other studies SMD was accomplished with phycobiliproteins.[3–4] Single-molecule detection was reported in the late 1980s at liquid helium temperature[5] or for trapped atoms,[6–7] which are conditions not suitable for biochemical experiments. In this chapter we will focus mainly on SMD of single fluorophore molecules or a larger molecule containing a single bound fluorophore under typical conditions used for biochemical experiments.

There are several methods for detection of single or small numbers of fluorophores. Fluorescence correlation spectroscopy (FCS) measures fluctuations in the small number of molecules in a focused laser beam. FCS will be described in the following chapter. FCS is useful with freely diffusing molecules. Other methods for SMD are based on optical imaging using various forms of microscopy. Using these methods a molecule can only be imaged if it stays in one place during observation. Hence spectroscopic studies of single molecules are almost invariably performed on immobilized molecules. This can be accomplished with highly viscous or rigid polymers or with molecules tethered to a surface.

SMD is an exciting methodology for several reasons. From a fluorescence point of view we begin to deal with absolute quantities rather than relative intensity values. When performing anisotropy measurements on single molecules the theory changes because the classic equations for anisotropy (Chapter 10) were derived based on averaging of the signal from a large number of randomly oriented molecules. Perhaps the dominant reason for using SMD is to avoid ensemble averaging. For instance, suppose a solution contains two types of fluorophores. The emission spectra of a single molecule in the mixture will be representative of just one type of molecule, and not an average spectrum. Single-molecule studies of enzymes can reveal the time course of the enzymatic reaction, without the use of high-speed mixing or other synchronization methods that are needed when studying a large number (ensemble) of molecules. Structural fluctuations of macromolecules may be seen directly, which is not possible with ensemble-averaged measurements.

The usefulness of avoiding ensemble averaging is shown in Figure 23.1. Consider a molecular beacon that can exist in a closed state that is quenched or an open state that is fluorescent. Assume that the temperature is adjusted so that half the molecules are closed and half are open. The ensemble spectrum from a solution containing many molecular beacons would have an intensity 50% of the maximum unquenched intensity (lower panel). This ensemble spectrum would not reveal if half of the beacons are open or closed, or if all the beacons are 50% quenched. Emission spectra of the single molecules would provide this informa-

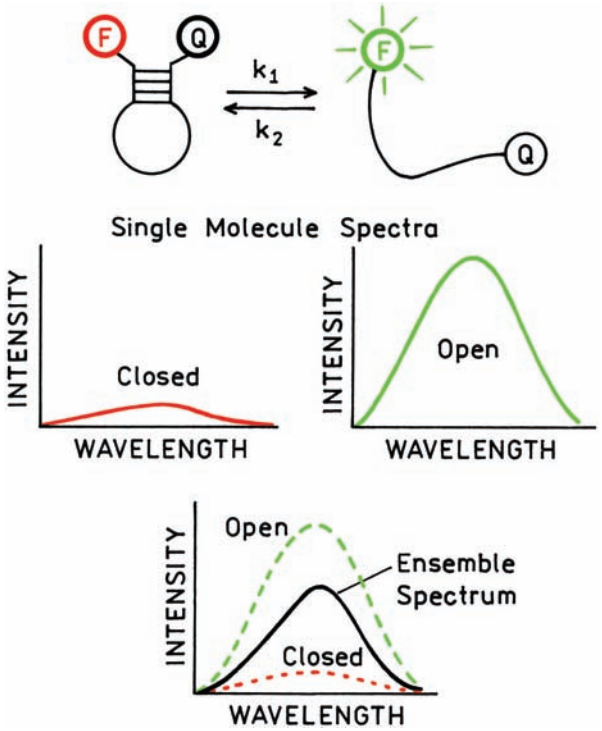

Figure 23.1. Comparison of single-molecule and ensemble emission spectra for a molecular beacon.

tion. If the observed single-molecular beacon were open the single-molecule spectrum would have the intensity expected for a single fluorophore. If the observed molecular beacon were closed, it would display a lower intensity or would not be observable. Intermediate intensities would be observed if the beacon was partially quenched. If the molecular beacon folds and unfolds on the timescale of the measurements then the signal would fluctuate. This example shows how observation of single molecules can reveal information about the conformation of biomolecules which is not available when observing many molecules.

Another opportunity using SMD is to study reaction kinetics without synchronization of the reaction. Consider an enzyme catalyzed reaction where the substrate is nonfluorescent and the product is fluorescent. The reaction is usually started by addition of the substrate (Figure 23.2, top panel) and the progress of the reaction followed by the change in fluorescence intensity. These data would not reveal any intermediate steps in the reaction. Now consider an experimental design where a single enzyme molecule is bound to a surface. In this case the enzyme (E) is labeled with a fluorophore (F) and the substrate contains a quencher. When the substrate (S–Q) binds to the enzyme

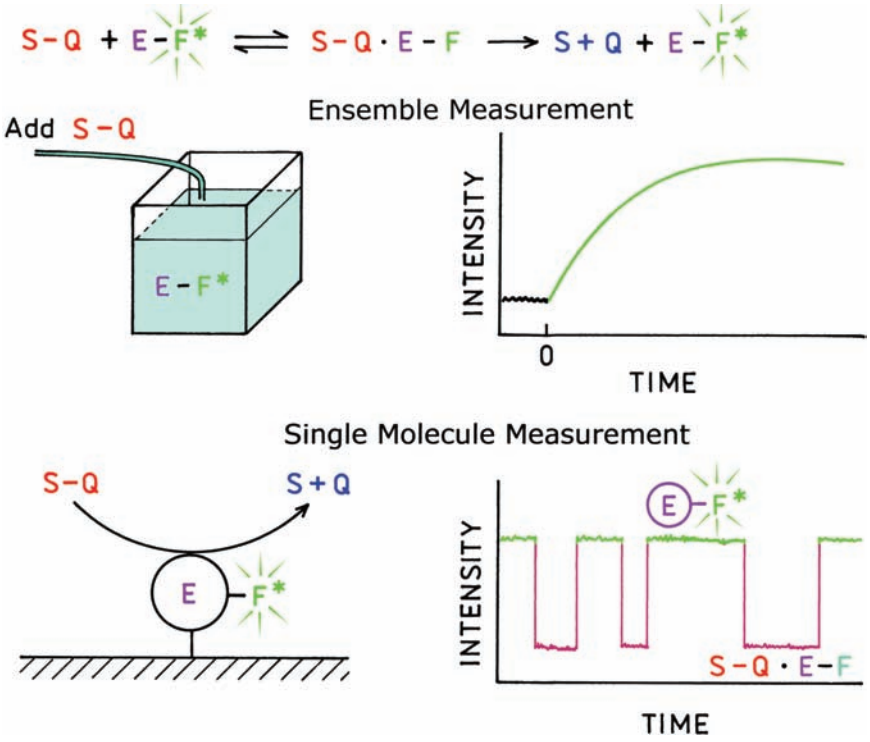

Figure 23.2. Comparison of ensemble and single-molecule enzyme kinetics. The enzyme is labeled with a fluorophore (F). The substrate contains a group (Q) that quenches the fluorophore.

the intensity of F decreases (lower panel). When the product dissociates the intensity will return to the initial value. If intermediate states are present they might be observed by intermediate intensities. The time intervals when the intensities are high or low can be used to determine the rate constants for the reaction. In the case of the single molecule it is not necessary to consider the starting time for the reaction. The reaction can be studied in a stationary experiment, assuming the substrate concentration is not changing. Measurements on different single enzyme molecules would reveal if there were subpopulations with different kinetic constants. These two examples (Figure 23.1 and 23.2) show that a wealth of new information is available when observing single molecules.

Perhaps surprisingly, SMD is not presently used for high-sensitivity detection. Single molecules are observed but not usually counted. At present it is considerably easier to find and measure single immobilized molecules than to count the number of molecules in a sample. However, single-molecule counting is likely to be used more frequently in the future, as shown by attempts to determine the sequence of single strands of DNA.[8–9] The field of SMD is growing rapidly. We have attempted to provide a snapshot of this changing technology. More detail abut SMD can be found in recent reviews and monographs.[10–18]

23.1. DETECTABILITY OF SINGLE MOLECULES

It is informative to consider the samples and instrumental requirements needed to detect the emission from a single molecule above the background signal from the system. In any real system there will be background signal due to impurities in the sample, emission from optical components, scattered light at the incident wavelength, and dark counts (dark current) from the detector. Assume for the moment that the instrument is perfect without signal from these sources. Surprisingly, even a perfect instrument does not guarantee that a single fluorophore can be detected. If one examines the literature on SMD one finds that SMD is almost always performed in a restricted volume, that is, by observing a small region of the sample. This restriction is a consequence of intrinsic Raman scattering, which cannot be avoided.

Rhodamine 6G (R6G) is frequently used for SMD. Figure 23.3 shows the emission spectrum of R6G along with the Raman spectrum of the solvent ethylene glycol.[19] The optical cross-section of a chromophore (σ) can be calculated from its molar extinction coefficient (ε) using[16]

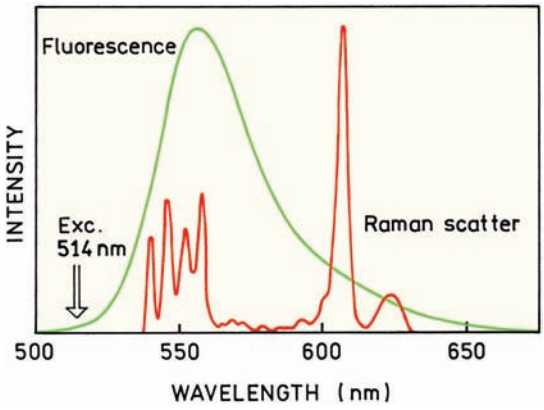

Figure 23.3. Emission spectrum of rhodamine 6G in ethylene glycol. Also shown is the Raman spectrum for ethylene glycol. Revised from [19].

$$\sigma_A = 2.303\,\varepsilon/N \qquad (23.1)$$

where N is Avogadro's number. The electronic transition of R6G is strongly allowed and the cross-section for absorption (σ_A) is essentially equal to its geometric cross-section, about 4 x 10^{-16} cm^2, or 4 $Å^2$. For a single molecule of ethylene glycol (EG) the cross-section for Raman scattering is about 3 x 10^{-28} cm^2, or 3 x 10^{-12} $Å^2$.[19] Since the Raman signal appears in the same wavelength range of R6G fluorescence, the contribution of Raman scatter cannot be completely eliminated by emission filters. The Raman scatter from the ethylene glycol solvent will equal the emission from R6G when one R6G molecule is dissolved in 1.3 x 10^{12} molecules of EG. Since one mole of EG occupies about 56 ml, this number of molecules occupies a volume of 1.2 x 10^{-10} ml or 120 μm^3. In order to obtain a signal from R6G equal to the Raman scatter the molecule must be in a square less than 4.9 µm on each side. Raman scatter, from the solvent limits the detectability of signal fluorophores to volumes of less than about 100 fl. Single-molecule experiments are usually designed so that the observed volume surrounding a single fluorophore is about 1 femtoliter (10^{-15} l), which is the volume of a cube 1 µm on each side.

The difficulty of SMD can be seen by considering a single R6G molecule in 1 ml of water (Figure 23.4). Assume that the quantum yield of R6G is unity and that the spatial distribution of the emission and scattered light is similar. The signal observed for each molecule will be proportional to its cross-section and the number of molecules.

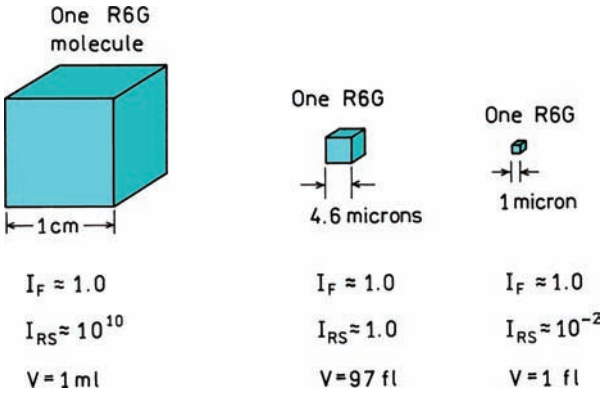

Figure 23.4. Intensities of Raman scattering from water relative to a single R6G fluorophore.

Assume the Raman cross-section for water is 10^{-28} cm^2. One ml of water contains 3.3 x 10^{22} molecules, so that the Raman scatter from 1 ml of water is the product of the Raman cross-section (σ_S) and the number of molecules, or about 3 x 10^{-6} cm^2. The Raman scatter from 1 ml of water is 10^{10}-fold greater than the signal from one R6G molecule. Without some breakthrough in technology a single fluorophore in a milliliter volume cannot be detected.

While SMD is difficult, the situation is not hopeless. In order to obtain signal from the fluorophore, comparable to or greater than from the solvent, the size of the observed sample has to be restricted. For example, in order to make the emission of one R6G equal to that of the solvent water the volume has to be reduced by a factor of 10^{10} to 10^{-10} cm^3. This volume corresponds to a box 4.6 μm on each side (Figure 23.4). Of course, for a useful experiment the signal has to be larger than the scatter. To make the emission 100-fold larger than the scatter the volume has to be reduced to 10^{-12} cm^3, which corresponds to a box 1 micron on each side, which is 10^{-15} l = 1 fl. Modern microscope objectives easily focus light to wavelength dimensions, which for 600 nm light would be about 0.22 fl. Hence, based on consideration of only Raman scatter, it should be possible to detect single fluorophores using microscope objectives. In reality the situation is far less favorable because all the molecules in the light path of the microscope contribute to the signal. Confocal optics are needed to reduce the observed volume by rejecting signal from above and below the focal plane. The solvent or sample may contain fluorescent impurities; the detectors always have dark counts. Additionally, single molecules often photobleach while they are being observed. SMD is still a technological challenge.

23.2. TOTAL INTERNAL REFLECTION AND CONFOCAL OPTICS

23.2.1. Total Internal Reflection

Prior to describing the optical methods needed for SMD it is necessary to understand the principles used to restrict the observed volume. One commonly used method is total internal reflection (TIR). TIR occurs when a beam of light encounters an interface with a lower refractive index on the distal side, and the angle of incidence exceeds the critical angle (θ_C). The underlying physics of TIR is somewhat complex[20–23] but the end result is simple. Consider a hemicylindrical prism (n_2) optically coupled to a slide with the same refractive index n_2 (Figure 23.5), and assume light is incident at an angle θ_I. Assume the sample has a lower refractive index n_1. The values of n_2 = 1.5 and n_1 = 1.3 are typical of glass and water, respectively. If one examines the intensity of the transmitted light one finds most of the light is transmitted at low angles of incidence. The reflectance is above zero when values of θ_I are less than 60° (lower panel). For angles greater than the critical angle θ_C, the transmission drops to zero and the reflectivity increases to 100%. For $\theta_I > \theta_C$ the beam is said to be totally internally reflected. The critical angle can be calculated from n_1 and n_2 using

$$\theta_C = \sin^{-1}\left(\frac{n_1}{n_2}\right) \tag{23.2}$$

For $\theta_I > \theta_C$ the beam is completely reflected at the interface, but the incident beam can still interact with the sample at the glass–water interface. This is because when TIR occurs the intensity penetrates a short distance into the sample. The intensity of the light along the z-axis, the square of the electric field, is given by

$$I(z) = I(0)\exp(-z/d) \tag{23.3}$$

where $I(0)$ is the intensity at the interface. The decay constant is given by

$$d = \frac{\lambda_0}{4\pi}(n_2^2 \sin\theta_2 - n_1^2)^{-1/2} \tag{23.4}$$

where λ_0 is the wavelength of the incident light in a vacuum. For 600-nm light with the parameters in Figure 23.5

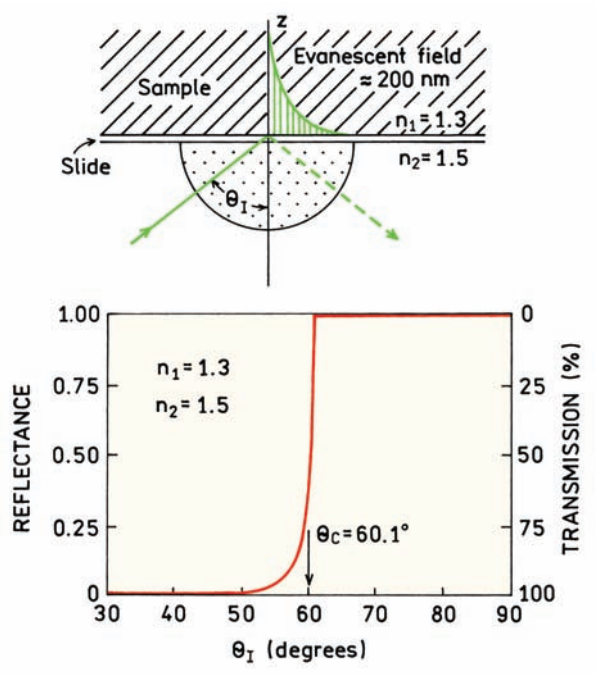

Figure 23.5. **Top**: Optical geometry for total internal reflection (TIR). **Bottom**: Calculated reflectance and transmittance for n_2 = 1.5 and n_1 = 1.3.

and an incidence angle of 70° one finds d = 73.3 nm. The values of d are typically a fraction of the wavelength. Equation 23.4 is sometimes defined incorrectly in various publications, and describes the distance-dependent decreases in intensity. Equation 23.4 is sometimes presented with a factor of 2π in the denominator rather than 4π. The expression with 2π in the denominator represents the distance-dependent decrease in the electric field, not the intensity.

Total internal reflection is valuable in SMD because it provides a way to limit the volumes. When using TIR only fluorophores within the evanescent field are excited. Instead of a long illuminated path through the sample, the effective illuminated path is sub-wavelength in size. The restricted illuminated distance along the z-axis reduces the effective volume and makes it possible to detect single molecules. This can be seen by calculating the volume of a spot illuminated using TIR conditions. Suppose the spot size is 20 μm in diameter and the penetration depth is 100 nm. The effective volume of the illuminated region is about 30 μm^3 = 30 fl. Hence a single molecule of R6G should be detectable using these conditions, with a signal-to-noise ratio (S/N) near 3 when observing the entire volume. If the observed volume is reduced further the S/N ratio will be improved.

23.2.2. Confocal Detection Optics

Figure 23.4 demonstrated the need to decrease the effective sample size in order to detect a fluorophore above intrinsic scatter from the sample. It would be difficult to prepare such a nano-sized structure containing a single fluorophore. Even if one could prepare a small volume with a single fluorophore this would not be useful because the goal is usually to select and observe a region from homogeneous solutions or heterogeneous biological samples. Fortunately, confocal fluorescence microscopy provides an optical method to limit the observed volume.

Figure 23.6 shows a schematic of confocal optics. The principles have been described in more detail in many reports.[24–27] Suppose the sample is thicker than a single layer of fluorophores, such as a polymer film containing a low concentration of fluorophores. Illumination through the objective is called epi-illumination. The incident light excites all the fluorophores within the illuminated cone. Emission is collected back through the objective, which is called the epifluorescence configuration. Emission is separated from light at the incident wavelength by a dichroic filter that reflects wavelengths longer than the incident light to a detector. A dichroic filter is a device that transmits some wavelengths and reflects others. In this case the dichroic filter transmits the excitation and reflects the emission wavelengths.

When using single-photon excitation the incident light excites the entire thickness of the sample with a cone-like

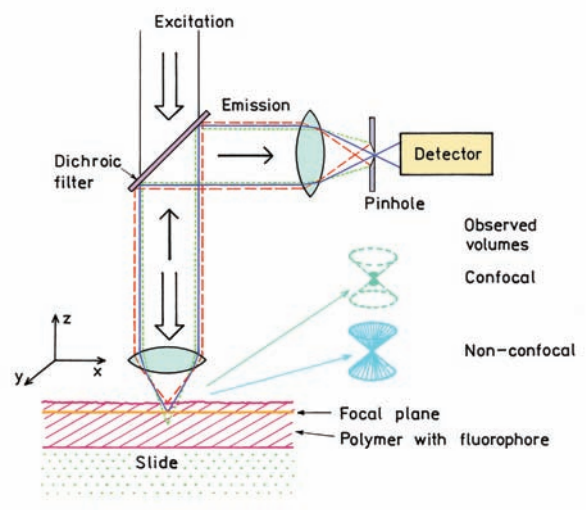

Figure 23.6. Principle of epifluorescence with confocal detection.

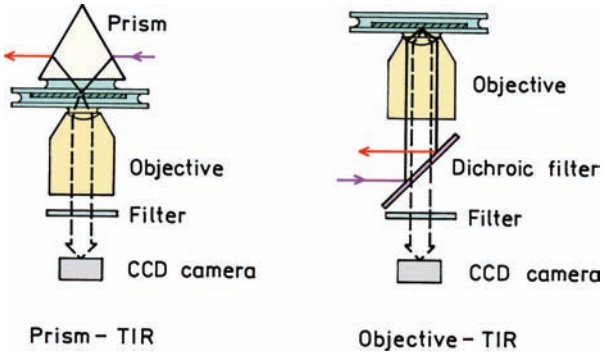

Figure 23.7. Optics for SMD imaging based on total internal reflection. Revised from [16].

pattern (Figure 23.6). The objective will collect the light from this cone, which includes the signal from the fluorophore, Raman scatter from the solvent, and emission from impurities in the solvent. If a single fluorophore is present in the illuminated cone its emission can be overwhelmed by the background from the solvent because the observed volume is too large. Suppose the laser beam is focused to a diameter of 500 nm and the sample is 100 μm thick. Then the observed volume is about 20 fl, which is borderline for single-molecule detection.

The difficulty due to unwanted signal from the solvent can be solved to some extent using confocal optics. This means that a small pinhole aperture is placed at a focal point in the light path. By ray tracing of the light path one can see that light from above or below the focal plane is not focused on the pinhole, and does not reach the detector. Using this approach the effective depth of the sample can be reduced to about twice the incident wavelength. The z-axis resolution is typically several-fold less than the resolution in the x–y focal plane. Suppose the effective observed volume is a cylinder 500 nm in diameter and 1000 nm long. The volume of the cylinder is about 0.2 fl. Using Figure 23.4 one sees that the signal from a single fluorophore can be about 500-fold larger than the Raman scatter. This is a very optimistic estimate of the S/N ratio, which does not include a number of factors, including impurities, nonideal properties of the lenses and filters, photobleaching, and saturation of the fluorophore.

23.3. OPTICAL CONFIGURATIONS FOR SMD

Essentially all SMD instruments use an optical configuration which limits the observed volume. Different approaches are used for wide-field observations and point-by-point observations. For wide-field observations the most common approach is to use TIR. Two commonly used wide-field approaches[16,28] are shown in Figure 23.7. Both configurations are based on an inverted microscope. The most direct approach (left) is to excite the sample through a prism so that the excitation undergoes TIR. Fluorophores in the sample, which are also within about 200 nm of the interface, are excited by the evanescent field. The emission is collected by an objective, filtered to remove unwanted light, and imaged on a low-noise CCD camera. When using this approach it is necessary to aim the incident light at the focal point of the objective.

A somewhat more convenient approach to TIR illumination is shown on the right side of Figure 23.7. In this case illumination occurs around the sides of the objective, causing the light to be incident on the glass–water interface at an angle above the critical angle. This creates an evanescent field that excites a thin plane of the sample next to the interface. With this configuration the excitation light is always aligned with the collection optics because the excitation and emission pass through the same objective.

It is informative to examine a single-molecule image. Figure 23.8 shows an image of a mutant T203Y of green fluorescent protein (GFP).[16] This image was obtained using the prism and TIR configuration with a CCD detector. The GFP molecules were immobilized in dense poly(acrylamide) to prevent translational diffusion during the 100 ms exposure time. If the molecules were not immobilized they would diffuse several microns during this time and not be seen in the image. The single-molecule intensities are not all the same, which is due in part to the decaying evanescent

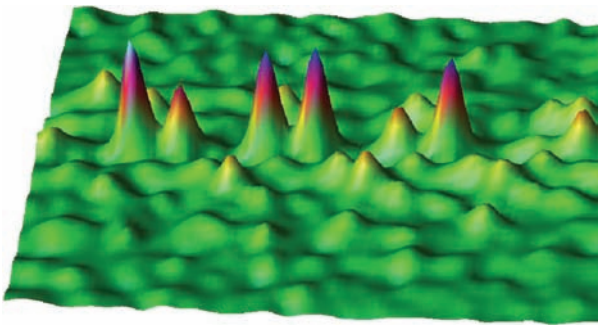

Figure 23.8. Single-molecule image of GFP mutant T203Y. The image was obtained using TIR illumination and a CCD camera. The GFP mutant was immobilized in poly(acrylamide). The image is 2.4 x 2.4 μm. Images courtesy of Dr. W. C. Moerner from Stanford University.

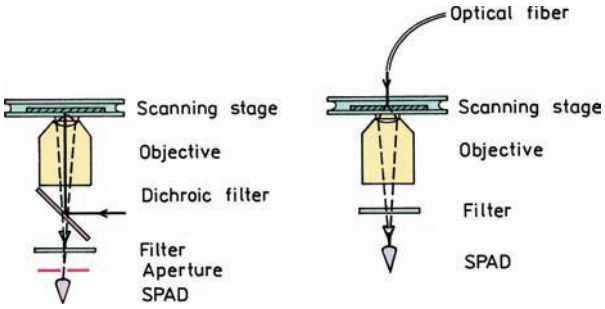

Figure 23.9. Optics for SMD using point-by-point measurements. Revised and reprinted with permission from [16], Copyright © 2003, American Institute of Physics.

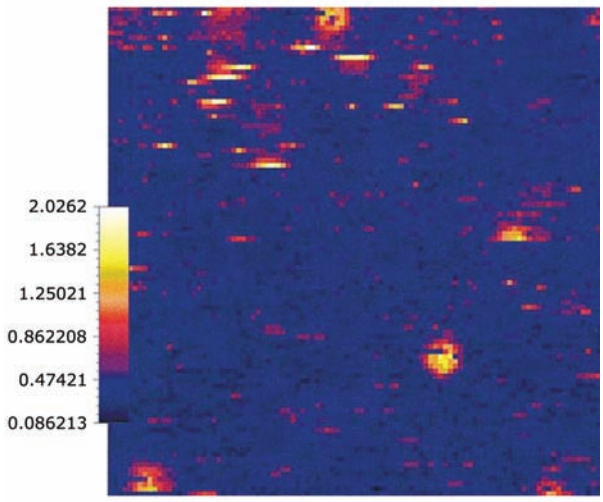

Figure 23.10. Confocal fluorescent images of single molecules of GFP mutant 10C in poly(acrylamide) measured by stage scanning. Image size 10 x 10 μm. Reprinted with permission from [32].

field and different distances of the GFP molecules from the glass–polymer interface. As we will describe below, single molecules often show blinking behavior. Blinking is not seen in the images because the CCD is an integrating detector that measures total intensity during the data collection time. The diameter of each single-molecule image is about 200 nm, which is much larger than the size of the GFP or its chromophore. The size of the spots is determined by the resolution of the optics.

Another approach to limiting the observed volume for SMD is to use confocal optics[29–31] and point-by-point detection, rather than imaging. Two configurations for point-by-point SMD measurements are shown in Figure 23.9.[16] The left side shows a confocal configuration with objective illumination. There is a single-point detector so the sample is not directly imaged. Instead, a single point is observed at one time. The sample stage is raster scanned to create an image. Fortunately, highly accurate motorized stages are available that provide resolution down to molecular sizes, or even less. For SMD the present detector of choice is a single-photon-counting avalanche photodiode (SPAD).

Figure 23.10 shows single-molecule images of a GFP mutant—10C—collected using confocal optics and stage scanning.[32] The size of the spots are about 500 nm in diameter, which is determined by the optical resolution and not the size of the molecules. The appearance of the images is dramatically different from the GFP images in Figure 23.8. These images were obtained by raster scanning so the same GFP molecule is illuminated several times. Some of the GFP molecules disappear completely on subsequent scans, and some molecules disappear in some scans but reappear in later scans. This occurs because the GFP molecules are blinking and/or photobleaching during the observation. Blinking occurs when the molecules undergo intersystem crossing to the triplet state. These molecules remain dark until they return to the ground singlet state. Blinking was not seen in Figure 23.8 because the CCD integrated all the emission occurring during the exposure time.

Another single-point approach to SMD and/or imaging is based on near-field scanning optical microscopy (NSOM). NSOM is based on a simple principle[33–35] but in practice is difficult. Highly localized excitation is obtained using an optical fiber (Figure 23.9 right). The end of the fiber is drawn to be very thin: typically 80 nm in diameter. The sides of the fiber are then coated with aluminum. Laser light is focused to enter the larger distal end of the fiber. A very small fraction of the light is transmitted from the tip of the fiber. Alternatively, the light in the fiber can be imagined as creating an evanescent field at the tip of the fiber, analogous to TIR. The tip is then positioned near the sample, typically with in 20 nm using components similar to an atomic force microscope (AFM). The fibers are fragile and the stage is usually scanned to create an image, while the fiber is held at a known distance above the sample. Because only a small region of the sample is excited, there is no need for a confocal aperture to eliminate scattered light from a larger volume of the sample.

Figure 23.11 shows a single-molecule NSOM image of the dye oxazine 720 in poly(methylmethacrylate) (PMMA). This image was obtained by scanning a metal-coated fiber above the surface, with illumination through the fiber. The

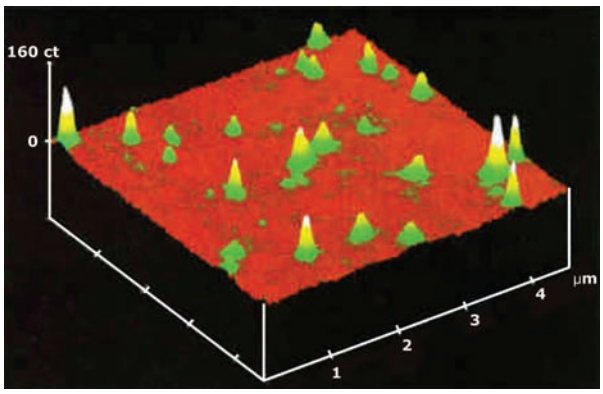

Figure 23.11. Single-molecule images of oxazine 720 in poly(methylmethacrylate) obtained using NSOM. Image size 4.5 x 4.5 µm. Revised from [13].

spatial resolution is not limited to optical resolution and is determined by the diameter of the fiber. In this image the spots are below 100 nm in diameter.

SMD imaging is also measured using laser scanning confocal microscopy (LSCM). LSCM is accomplished using optics similar to Figure 23.6. Instead of observing a single spot in the image, the laser excitation is raster scanned so that the focused light is scanned across the sample.[29–31] The light collected by the objective is focused on the pinhole to pass light from the desired volume element and reject light from outside the focal volume. A single-point detector, usually an SPAD, is used to measure the light returning from each point in the image.

Single-molecule imaging has been accomplished using standard epifluorescence and a high-quality CCD detector. This is possible if the sample is thin, where there is little or no signal from molecules outside of the focal plane. Figure 23.12 shows an epifluorescence image of a tetramethylrhodamine-labeled lipid (TMR-POPE) in a monolayer of POPC prepared as a Langmuir-Blodgett film.[36] Single molecules were observable because the sample was only the thickness of a phospholipid monolayer. This image illustrates the need for extremely low fluorophore concentrations for SMD. The mole fraction of TMR-POPE has to be below about 10^{-6} for single molecules to be observed because two fluorophores closer than the optical resolution of the microscope appear as a single spot.

23.4. INSTRUMENTATION FOR SMD

Prior to showing additional experimental results it is valuable to examine a typical instrument used for these measurements. Figure 23.13 shows the schematic for a confocal SMD instrument.[37] Laser light is brought to the sample by reflection off the dichroic filter. If needed, the polarization of the incident light is adjusted with polarizers and/or wave plates. Emission is selected by the same dichroic filter and then passes to the detectors. In order to find and/or image the fluorophores the stage is scanned in the *xy* direction,

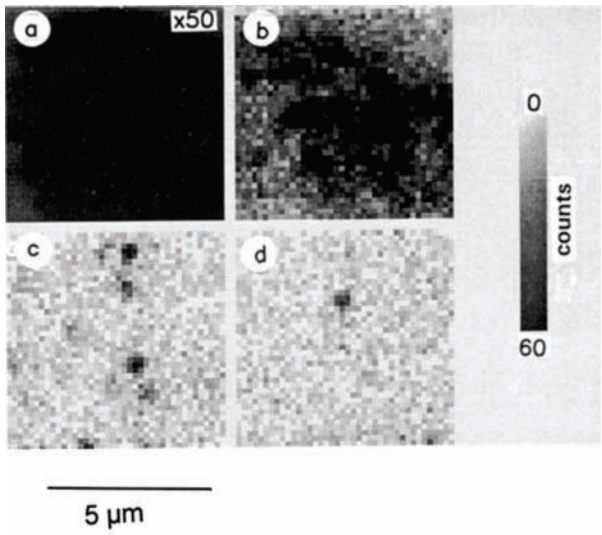

Figure 23.12. Epifluorescence images of TMR-POPE in a monolayer of POPC. The mole fractions of labeled lipid are (a) 6.5 x 10^{-3}, (b) 6.5 x 10^{-6}, (c) 6.5 x 10^{-8}, and (d) 6.5 x 10^{-9} mole/mole. In (a) the intensity was divided by 50. Exposure time was 5 ms. Reprinted with permission from [36]. Copyright © 1995, American Chemical Society.

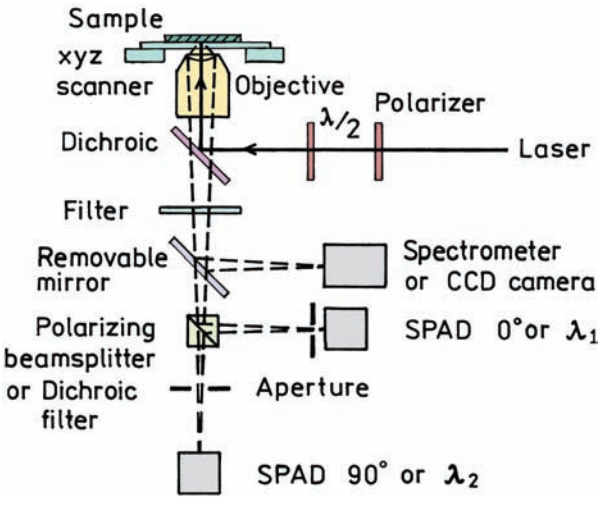

Figure 23.13. Schematic for stage-scanning confocal SMD. Revised and reprinted with permission from [37]. Copyright © 1998, American Chemical Society.

with z scanning if needed for focusing. The presence of a fluorophore is seen as a burst of photons when the fluorophore is in the incident beam. The most commonly used detector is the single-photon-counting avalanche photodiode (SPAD). The emission can pass through an aperture to provide confocality, or may just be focused on the SPAD allowing the small active area to serve as the aperture. In many measurements two SPADs are used, which allows measurements through different polarizer orientations or different wavelengths. If needed the emission can be directed toward a CCD camera for imaging, or a spectrometer for collecting emission spectra.

The instrumentation for single-molecule detection using NSOM is similar except that the excitation is delivered to the sample via a tapered metal-coated optical fiber (Figure 23.14). The fiber tips are fragile so there are usually feedback mechanisms to keep the fiber at a known distance above the sample. Because the sample is only excited near the fiber top there is no need for a confocal aperture to reduce background from out-of-focus regions of the sample.

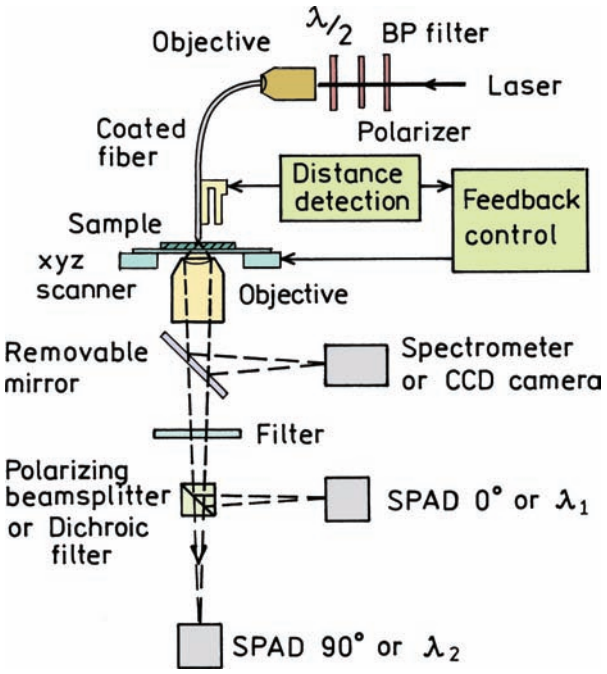

Figure 23.14. Schematic of a stage-scanning NSOM instrument for SMD. Revised and reprinted with permission from [38].

23.4.1. Detectors for Single-Molecule Detection

For single-point measurements on single molecules the presently preferred detector is the SPAD. At first glance it seems surprising to use an SPAD rather than a photomultiplier tube (PMT). PMTs are able to multiply single-photoelectron events by a million-fold. In contrast, a typical SPAD provides an amplification near 100-fold.[39] Essentially all single-point SMD experiments are performed using some type of single-photon counting (SPC) rather than analog detection. This is because the photon arrival rate is typically low so that individual photoelectron pulses are detectable. The use of SPC allows the lower threshold to be adjusted to neglect smaller noise pulses. It is possible to observe single-photon events with an SPAD, and there is no need for further amplification if the photon can be counted.

Single-photon counting can be accomplished using either a PMT or an SPAD. SPADs have several advantages over PMTs. One issue is that of simplicity. SPADs along with the electronics to count single-photon events are available in small packages that require only a 5-volt source. The higher voltages near 20 volts needed to drive the SPAD are obtained from internal circuits. In contrast, a PMT requires a much higher voltage—typically over 1000 volts for SPC. While small PMT high-voltage supplies are available, it is more difficult to create and shield these higher voltages.

Perhaps the main advantage of SPADs over PMTs is their quantum efficiency. As is described below, a single fluorophore can only emit a limited number of photons prior to photodestruction. This fact, and the limited total collection efficiency with a confocal microscope, makes it important to detect the incident photons with the highest possible efficiency. PMTs typically have quantum efficiencies near 20%. SPADs have efficiencies near 60% in the visible and up to 90% in the NIR. The quantum efficiencies of PMTs typically decrease at longer wavelengths. SMD is usually performed using red dyes because they have high extinction coefficients and because autofluorescence from the sample and apparatus is lower at the longer wavelengths. Hence SPADs provide a considerable quantum efficiency advantage over PMTs for SMD. SPADs also have a low rate of background count—25 to 100 counts per second—which is comparable to the best-cooled PMTs.

If SPADs are such efficient detectors, why are PMTs still the dominant detectors in fluorescence spectroscopy? An important advantage of PMTs is the large active area of the photocathode, which can be a square centimeter or more. As a result the emission does not need to be tightly focused to obtain efficient detection. Additionally, the high amplification of a PMT is an advantage in non-photon-counting applications. In contrast to PMTs, SPADs have

small active areas: typically near 200 µm in diameter. Such a small detection area would be inconvenient in a typical fluorometer, and most of the photons collected by the optics would fall on inactive regions of the SPAD. However, SMD is performed using confocal optics, so the emission is already focused to a small area, which can be on the active area of the SPAD. In fact, the SPAD itself can act like a pinhole because only the focal point of the optics falls in the active area.

For single-molecule imaging the detector of choice is the charged coupled device (CCD). A CCD contains an array of pixels, each of which acts like an individual detector.[40] A CCD is not a photon-counting detector, but it is an integrating detector. The signal in each pixel is proportional to the number of incident photons for as long as the CCD is active. Importantly, the noise in each pixel does not increase significantly with integration time, at least not with cooled scientific CCDs. There is a certain amount of noise associated with reading out the signal in each pixel, so that longer integration times are an advantage. Like SPADs, CCDs have a high quantum efficiency, especially at long wavelengths. The most detailed information on the performance of CCDs is usually provided by the camera companies.

23.4.2. Optical Filters for SMD

In single-molecule detection it is essential to reject scattered light at the excitation wavelength. Fortunately, high-quality optical filters are available for this purpose. Depending on their method of production they may be called holographic notch filters or Rugate notch filters.[41–42] Figure 23.15 shows the absorption spectra of typical notch filters. These filters transmit all wavelengths except a narrow band at the wavelength that needs to be rejected. The optical densities at these wavelengths can be very high—4 to 6—with half-widths of 10 to 20 nm.

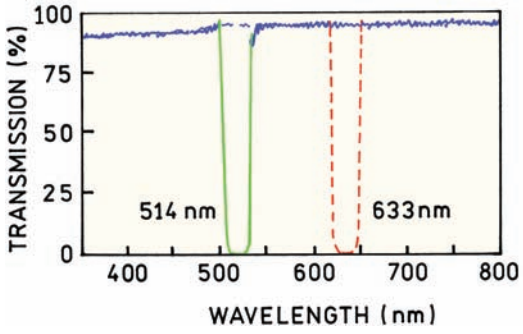

Figure 23.15. Transmission profiles of laser notch filters.

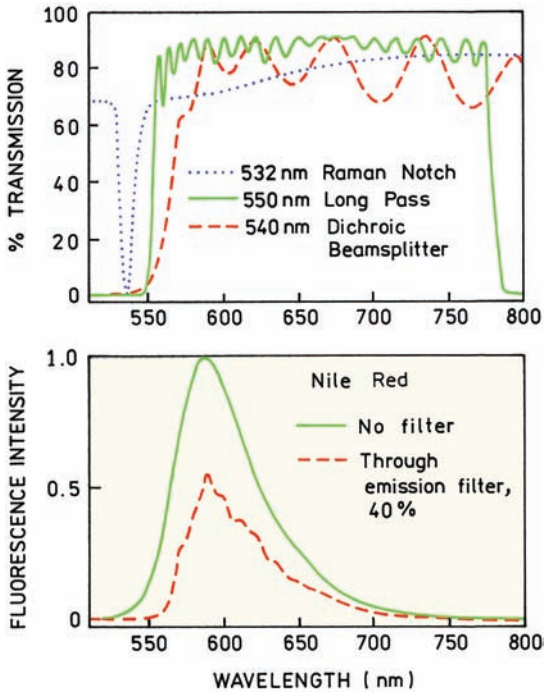

Figure 23.16. Emission filters and emission spectra of Nile Red in methanol. Revised from [16]. Revised and reprinted with permission from [16], Copyright © 2003, American Institute of Physics.

In single-molecule experiments extreme care is needed to eliminate scattered light, so that selection of emission filters is critical. Because of the intense illumination used for SMD the Rayleigh scattered excitation needs to be attenuated by a factor of 10^7 to 10^8-fold. Figure 23.16 (top panel) shows a combination of filters selected to observe Nile Red using 532-nm excitation. The Rayleigh scatter is rejected by a combination of three filters: a notch filter, a dichroic filter, and a longpass filter.[16] By careful selection of the filters the desired emission was attenuated only twofold (lower panel).

Figure 23.17 shows images of the fluorophore $DiIC_{12}$ that was spin coated on glass from a toluene solution.[43] If the initial solution is too concentrated the signals from the molecules overlap, resulting in a spatially continuous intensity (left). At a lower initial concentration, individual $DiIC_{12}$ molecules can be seen (middle), and at lower concentrations only few molecules are seen (right). The spots for a single molecule are about 300 nm across, reflecting the limited resolution available with light microscopy. The bright spots were assigned to single molecules based on the pro-

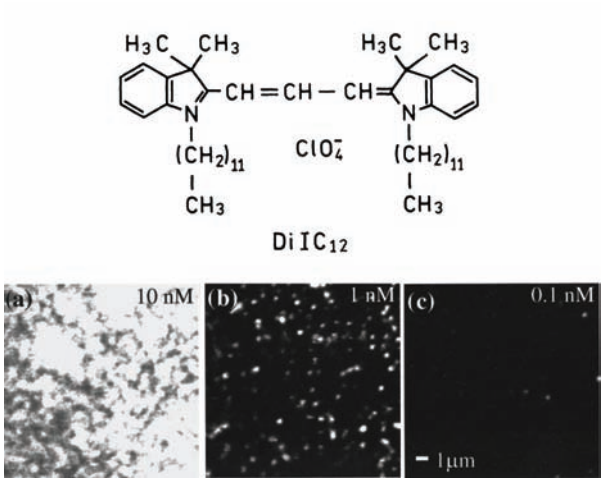

Figure 23.17. Single-molecule images of $DiIC_{12}$ on glass obtained using the stage-scanning configuration shown in Figure 23.13. Revised and reprinted with permission from [43], Copyright © 1998, American Institute of Physics.

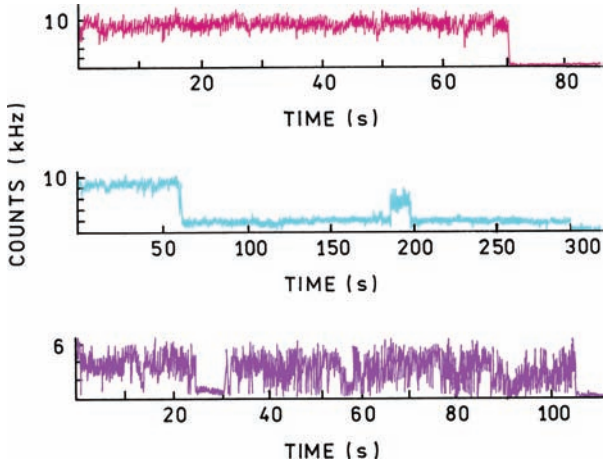

Figure 23.18. Time-dependent intensities of $DiIC_{12}$ on glass. Revised and reprinted with permission from [43], Copyright © 1998, American Institute of Physics.

portionality of number density to concentration and observation of single-step photobleaching. The different intensities for the various single molecules are thought to be due to different orientations of the fluorophore relative to the polarized incident light.

Close examination of the middle panel in Figure 23.17 shows that some of the single-molecule spots are half-circles rather than circular. This result shows an important aspect of SMD, all the fluorophores display blinking. Examples of the blinking are shown in Figure 23.18 for three different $DiIC_{12}$ molecules. In each case the intensity fluctuates dramatically, and eventually the emission stops when the molecule undergoes permanent photodestruction. The middle panel is the most typical blinking profile: a relatively constant intensity, followed by a rapid drop in intensity, followed by a return of the intensity. This blinking phenomenon explains the half-circles in Figure 23.17. Recall that the stage is scanned in the x and y directions to create the image. A single molecule is illuminated several times as the sample is raster scanned through the laser beam. If the fluorophore undergoes blinking or destruction during this somewhat continuous illumination it is not seen in the subsequent line scans, resulting in the partial circles. This illustrates an important advantage of stage scanning with SPADs. One can follow a single molecule in time to obtain a more detailed view of its photophysical behavior.

An important feature of SMD is the ability to examine the behavior of a single molecule rather than the average behavior of numerous molecules. This property is revealed by the emission spectra for individual molecules of $DiIC_{12}$ (Figure 23.19). These spectra are not for the same molecules used for Figure 29.18. Different emission spectra were found for different molecules. Often the single-molecule spectra were the same as the bulk phase spectra (lower left and dashed). However, the spectra of single molecules can also be dramatically different (right panels). These spectral changes can be the result of a number of mechanisms, such as different local environments on the glass. The behavior of the molecules depends upon the composition of the sample. The blinking and spectral changes are usually different for fluorophores on glass or embedded in a polymer. In the case of $DiIC_{12}$ in PMMA, different emission spectra were observed for the same fluorophore at different times,[16] a phenomenon called spectral diffusion. The important point is that SMD can provide resolution of underlying molecular heterogeneity, which can be due to either the local environment of the fluorophore or the conformational heterogeneity in macromolecules.

Single-molecule images of DiI-C_{18} embedded in poly(methylmethacrylate) were also observed using NSOM.[44] The excitation was circularly polarized to provide equal excitation of each fluorophore irrespective of the dipole orientation around the z-axis. The emission was passed through a polarizing beamsplitter to separate the polarized components and sent to separate SPAD detectors. The spots are color coded to show the dipole orientation, which was determined by the relative intensities of each polarized component (Figure 23.20). It is interesting to notice that single molecules display polarized emission, even if the

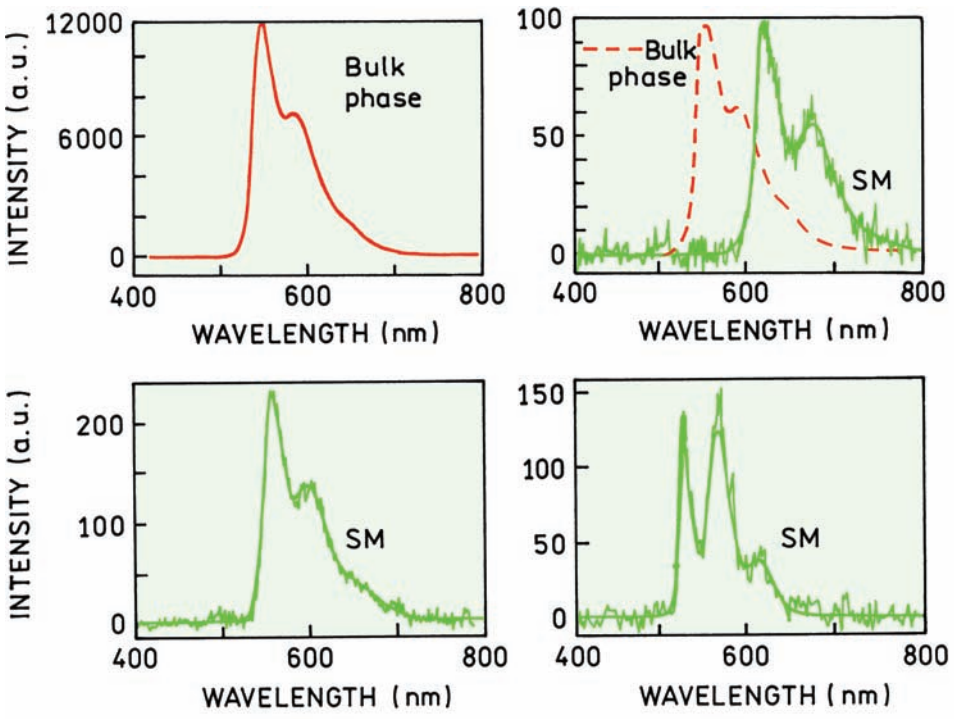

Figure 23.19. Emission spectra of single molecules of $DiIC_{12}$ on glass. These spectra are not from the same molecules used for the time-dependent traces in Figure 23.18. The spectrum in the upper left is from a bulk phase solution. SM, single molecule. The dashed line in the upper right is the bulk phase emission, normalized with the SM emission. Revised and reprinted with permission from [43], Copyright © 1998, American Institute of Physics.

excitation along the *z*-axis is unpolarized. This occurs because the dipole in the rigid polymer has a unique orientation. If a fluorophore is excited it will emit according to its orientation, and not the polarization of the incident beam. Additionally, the polarization can be greater than 0.5, or the anisotropy greater than 0.4, because the maximum polarization or anisotropy of a single dipole along an axis is 1.0 (Chapter 10). The extent of excitation is complex because the near field at the fiber top is more complex than simple linear polarization.[45–46]

23.5. SINGLE-MOLECULE PHOTOPHYSICS

When observed with high illumination intensities almost all fluorophores display blinking. This blinking by single fluorophores can be explained by a simple photophysical model.[47–50] The dominant origin of fluorophore blinking is thought to be intersystem crossing (isc) to the triplet state (Figure 23.21). In this Jablonski diagram the wide arrows are intended to represent high rates of excitation and emission, which is typically the case when detecting single molecules. The incident intensity has to be high enough to result in a rate of detected photons that is higher than the dark count of the detector. Increased incident intensities will not increase the signal-to-noise ratio if the background signal is due to autofluorescence from the sample, because this component will also increase with increases in incident intensity.

The origin of fluorophore blinking can be understood from the kinetic equations describing the population of the S state. The steady-state solution of these equations yields the dependence of S_1 on the rate constants in Figure 23.21. The number of molecules in the first singlet state is given by

$$S_1 = \frac{\sigma I_e S_T}{\tau^{-1} + \sigma I_e (1 + k_{isc}/k_{ph})} = \frac{\tau \sigma I_e S_T}{1 + I_e/I_s} \qquad (23.5)$$

The rate of excitation is proportional to the excitation intensity I_e and the cross-section for absorption σ. S_T is the total number of fluorophores and τ is the lifetime. The S_1 population will show a hyperbolic dependence on the incident

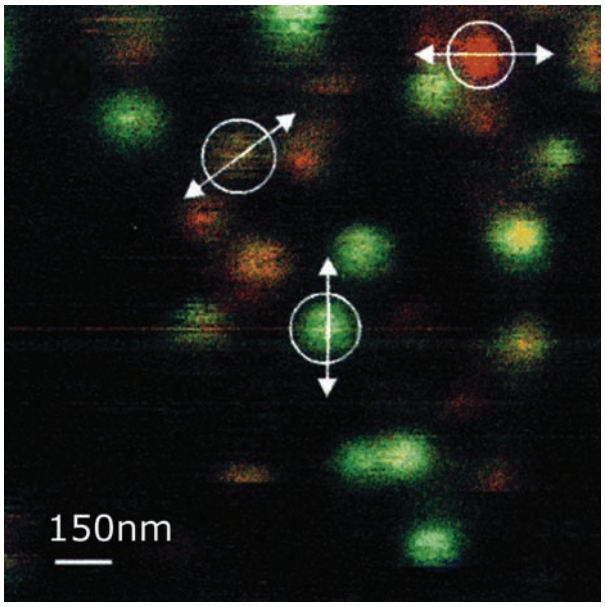

Figure 23.20. NSOM single-molecule imaging of DiI-C_{18}. The colors represent the emission dipole orientation, red horizontal 0°, green vertical 90°, yellow equal signals in both channels. Reprinted with permission from [44].

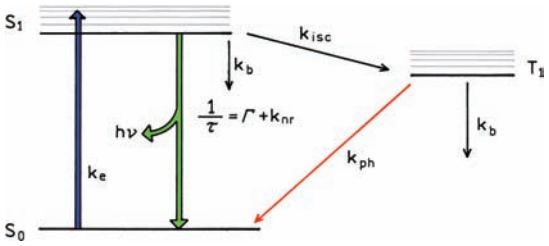

Figure 23.21. Jablonski diagram for single-molecule blinking. The wider arrows are intended to show high rates of excitation and return to the ground state.

intensity I_e. Equation 23.5 describes the entire population. If individual molecules are examined those in the triplet state are dark. The blinking properties of the fluorophore are determined primarily by the rate constants for crossing to the triplet state (k_{isc}) and for return from T_1 to the ground state (k_{ph}). It is likely that photobleaching (k_b) occurs from either the S_1 or T_1 state.

Figure 23.22 shows the photon count rate observed for a tetramethylrhodamine (TMR)-labeled lipid.[36] The numbers of photons per second initially increases linearly with incident intensity, but quickly reaches a saturating value. The laser intensities for SMD are typically rather high,

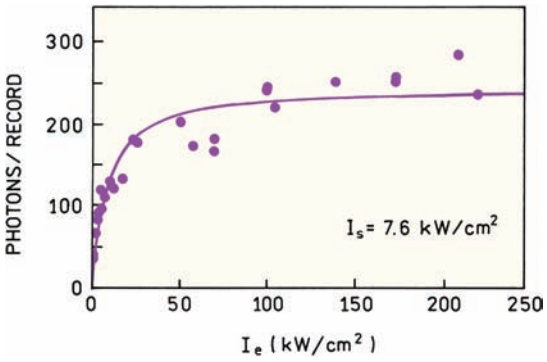

Figure 23.22. Laser intensity-dependent emission for a single lipid molecule labeled with TMR. Revised and reprinted with permission from [36]. Copyright © 1995, American Chemical Society.

which is needed to partially saturate the fluorophores and obtain a high photon emission rate. These conditions result in blinking and photodestruction photophysics of fluorophores. The general conclusion is that good fluorophores such as rhodamine can emit 10^5 to 10^6 photons prior to destruction. Many fluorophores are much less stable and may emit less than 1000 photons prior to bleaching. There is an interesting dilemma with regard to the effect of oxygen on photobleaching. On one hand it appears likely that oxygen can react with the excited states to destroy the fluorophore.[51–52] On the other oxygen quenching of T_1 should decrease the T_1 population, so the fluorophores will return more quickly to the ground state. Brighter single-molecule emission has been observed in the presence of oxygen, relative to an oxygen-free sample,[53] which was interpreted as due to the shorter lived T_1 state.

In addition to blinking the fluorophores also display irreversible photobleaching. The resistance of a fluorophore to photobleaching determines the average number of photons a fluorophore can emit prior to its destruction. The photostability of a fluorophore is described by its photobleaching quantum yield (ϕ_B) or the inverse ($\mu = \phi_B^{-1}$). The value of μ is the average number of excitation-relaxation cycles a fluorophore can undergo before photobleaching. When multiplied by the quantum yield, the product represents the average number of photons emitted by a fluorophore. Typical values of ϕ_B and μ are listed in Table 23.1 for representative fluorophores. These values are only rough estimates obtained by collecting data from several reports.[47–48] The number of cycles varies widely from 700 to 3 million depending on the fluorophore. These numbers are only guidelines because the actual number of cycles will

Table 23.1. Photostability of Representative Fluorophores[a]

Fluorophore	ϕ_B	μ
Carbostyryl 124	1.4×10^{-3}	700
Coumarin 139	1.2×10^{-3}	800
Coumarin 120	4.3×10^{-4}	2300
Cy5	5×10^{-6}	200,000
EGFP	8×10^{-6}	125,000
Fluorescein	3.8×10^{-5}	26,000
B-Phycoerythrin	8.8×10^{-6}	114,000
Rhodamine 6G	8.9×10^{-6}	112,000
Rhodamine 123	6.4×10^{-7}	1,600,000
TMR	2.6×10^{-6}	380,000
Texas Red	5.5×10^{-5}	18,200
TRITC	5.6×10^{-6}	179,000

[a]Representative vaues obtained from [47–48]. ϕ_B is the photobleaching quantum yield and $\mu = 1/\phi_B$. For some probes the averaged values are given.

vary widely depending upon the precise conditions of the samples such as the polymers and the presence or absence of oxygen.

23.6. BIOCHEMICAL APPLICATIONS OF SMD

23.6.1. Single-Molecule Enzyme Kinetics

Single-molecule detection provides an opportunity to follow a single enzyme molecule during its catalytic cycle. Suppose an enzyme molecule E is bound to the surface and labeled with a green-emitting fluorophore G (Figure 23.23), and that the substrate is labeled with a red-emitting fluorophore R. If one images the sample through a green filter there will be spots due to the immobilized enzyme. Except for blinking the green intensity will be constant. If the sample is imaged through a red filter there will be few if any red spots because the red fluorophores are rapidly diffusing. Occasionally the labeled substrate molecule will bind to the immobilized enzyme molecule. The immobilized red fluorophore will appear as a transient red spot. The duration of the red spot will depend on the time it takes for the substrate to bind, be cleaved, and then dissociate from the enzyme molecule. If a substrate analogue binds irreversibly the red spots will remain indefinitely until the fluorophore photobleaches. If the color images are overlaid the enzyme molecules with bound substrate will appear as yellow spots. The enzyme molecules without substrate will appear as green spots. Free substrates will not be seen as images due to their rapid diffusion.

Suppose the enzyme undergoes a conformational change upon binding substrate that increases the quantum

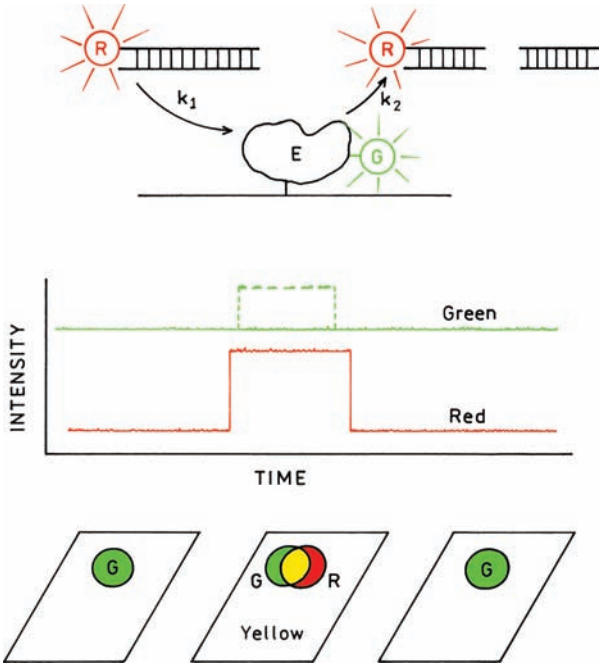

Figure 23.23. Schematic of a single-molecule enzyme-catalyzed reaction. The dotted line represents the case where the quantum yield of the green fluorophore increases upon substrate binding.

yield of the green fluorophore. In this case there will be an increase in the green intensity when the substrate binds (Figure 23.23, dashed line) and a return to the initial level when the substrate dissociates. The change in green intensity may correlate with the red intensity, or may exist for a shorter duration if a conformational change occurs after binding and before release of the substrate. Such a result would indicate the enzyme returns to its initial conformation before the products dissociate from the enzyme. Such a transient increase in green intensity would be difficult to observe in an ensemble measurement because only a small fraction of the enzyme molecules would be in the high-quantum-yield state at any given time. This description shows that considerable information can be obtained from measurements on single enzyme molecules.

23.6.2. Single-Molecule ATPase Activity

An example of single-molecule enzymatic activity is shown in Figure 23.24.[54] The S1 subfragment of myosin was bound to a glass surface using an albumin–biotin–avidin coating. The S1 subfragment possesses ATPase activity that cleaves the Cy3-labeled ATP. The protein was also labeled with Cy3, which allowed the single enzyme molecules to be located on the slide. After localization of the labeled

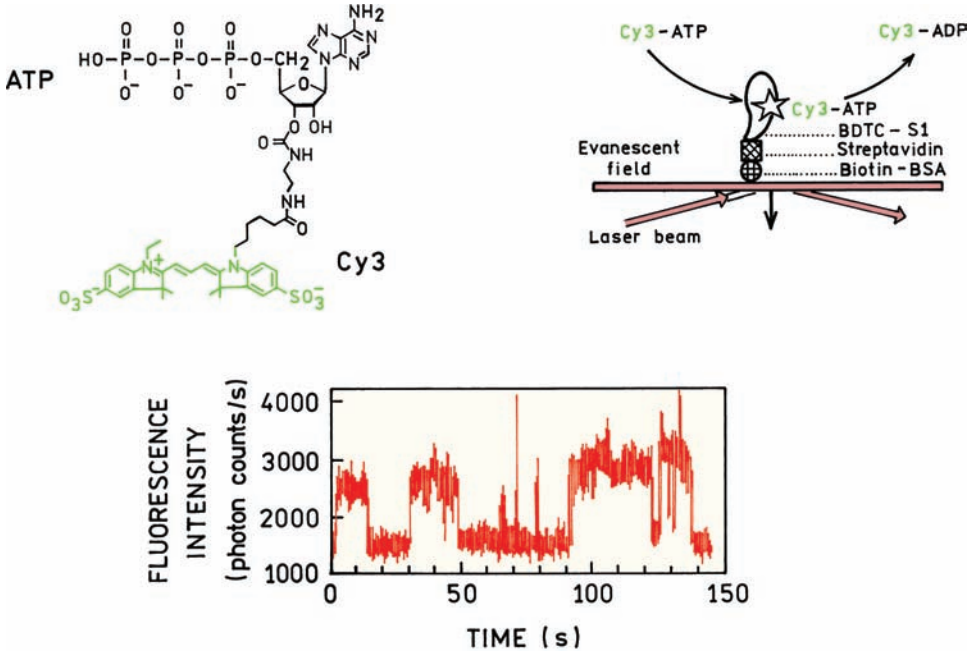

Figure 23.24. Single-molecule enzyme kinetics of ATPase activity. The enzyme was myosin subfragment 1 (S1). The measurements were performed using objective-type TIR. Reprinted with permission from [54].

ATPase the Cy3 bound to S1 was photobleached to eliminate its emission. This location was then observed after addition of Cy3-ATP. The intensity shows transient increases when Cy3-ATP/ADP is immobilized on the enzyme. The intensity returns to background when the Cy3-ADP dissociates from the protein. This experiment was performed using objective-type TIR. The small thickness of the illuminated area was important to reduce the background intensity from freely diffusing Cy3-ATP.

23.6.3. Single-Molecule Studies of a Chaperonin Protein

The concept shown in Figure 23.23 can be used to study any association reaction. Suppose the surface contains a green capture protein that binds to a red protein. Green dots will be seen whenever there is a capture protein. Red dots will only appear when this protein binds to the capture protein. Co-localization of green and red spots will indicate the presence of a complex on the surface. This concept has been applied to the study of chaperonin GroEL.

Chaperonins are a class of proteins that promote folding reactions in cells. They can facilitate folding of newly synthesized proteins or the refolding of denatured proteins. A well-known chaperonin is GroEL from (*Escherichia coli*). GroEL is a large cylindrical protein containing 12 subunits (Figure 23.25). GroEL was labeled with an indocyanine dye IC5 and bound to a glass surface.[55] Bovine (BSA) and human serum albumin (HSA) spontaneously

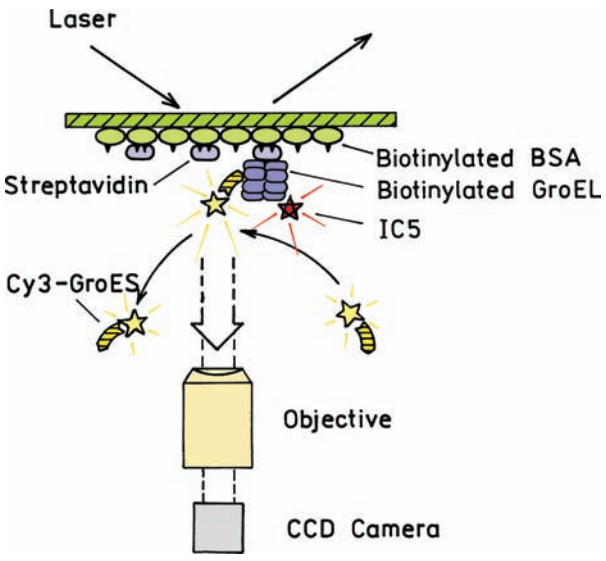

Figure 23.25. Chaperonin GroEL and GroES. GroEL is labeled with IC5 and GroES is labeled with Cy3. Reprinted with permission from [55].

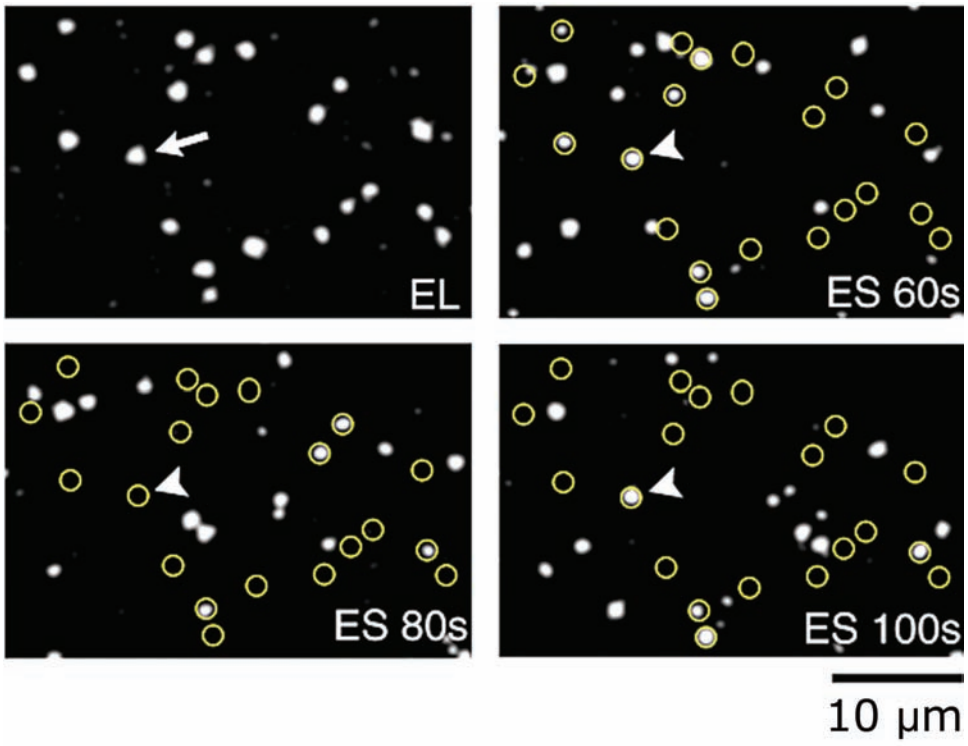

Figure 23.26. Single-molecule images from IC5-labeled GroEL (EL) and Cy3-labeled GroES (ES) at the indicated times. The images were obtained using TIR and an intensified CCD camera. The circles show the positions of GroEL. Reprinted with permission from [55].

bind to glass surfaces. If the BSA is biotinylated then avidin or streptavidin binds strongly to the surface. Streptavidin contains four biotin binding sites, providing residual binding sites for biotinylated GroEL. This method of attachment is frequently used to attach biomolecules to surfaces.

This system was examined using TIR excitation and an intensified CCD camera for imaging. The upper left panel in Figure 23.26 shows the locations of GroEL, as determined by emission from IC5. The remaining three panels show images of Cy3-GroES. In the presence of ATP GroES binds to GroEL and the complex acts to refold proteins. At first the images of GroES are confusing. Some appear where GroEL is also located and other GroES molecules appear where there appeared to be no GroEL. In either case the GroES has to be immobilized to see its emission. The different positions of GroES binding can be understood as due to molecular heterogeneity. The surface contains GroEL molecules that are labeled with IC5 and GroEL molecules that are not labeled with IC5. This shows how different types of reasoning are needed to interpret single-molecule and ensemble measurements.

The arrows in Figure 23.26 point to one GroEL molecule where a GroES molecule also binds. The GroES molecule appears in 2 of the 3 frames. In this case the absence of GroES in the 80-second frame is not due to blinking, but rather to dissociation from GroEL. The process of GroES binding to GroEL can be followed with time (Figure 23.27). The Cy3-GroES emission appears and disappears as it binds to and dissociates from GroEL. This observation of single-molecule binding kinetics provides a unique way to measure association and dissociation rates for the reaction. The times when GroES is observed and when it is missing provides a statistical measure of the rate constants. If a suitably large number of events are studied the fluctuations in Cy3-GroES emission can be used to determine the on and off rates for the reaction.

Histograms of the on and off times are shown in Figure 23.28. The top panel of Figure 23.28 shows a histogram of the off time, the time duration when emission from Cy3-labeled GroES is not observed. A large number of short-duration events were observed. A smaller number of events were observed for longer durations. This type of data can be

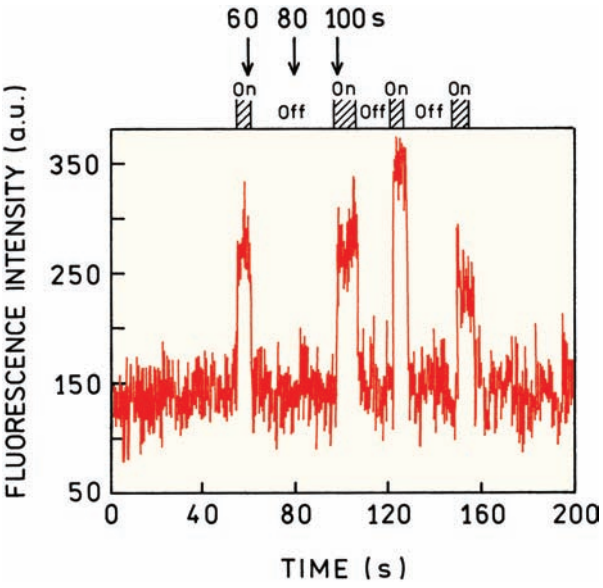

Figure 23.27. Time-dependent intensities of Cy3-labeled GroES for the spot indicated by the arrows on Figure 23.26. Reprinted with permission from [55].

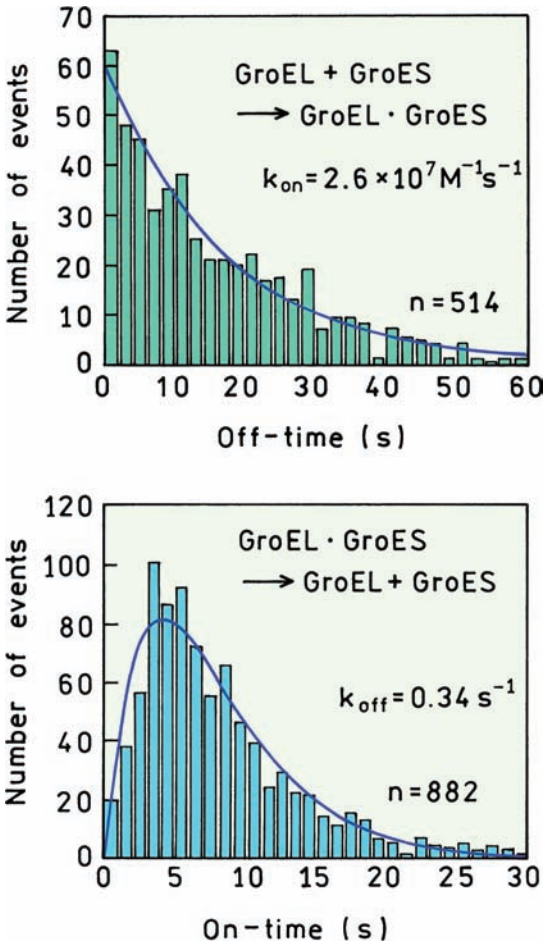

Figure 23.28. Histogram of the off (top) and on time durations (bottom) of GroES binding to GroEL. *N* is the number of events. The on and off times refer to the time duration when GroES contains, or does not contain, GroEL, respectively. k_{on} is the rate constant for the association reaction, k_{off} the rate constant for the dissociation reaction. Revised from [55].

used to calculate the rate constant for binding. Consider a single GroEL molecule that does not contain GroES. At short times there is a high probability that GroES is not bound. At longer times there is a smaller probability that GroES has not bound to GroEL. The histogram of the times needed for binding reveals the binding rate constant, just like the histogram in TCSPC reveals the lifetimes.

In a similar way the on times can be used to obtain the rate of GroES dissociation. Assume the starting point is the GroEL–GroES complex. We know the complex is present because of the emission from Cy3. The complex dissociates spontaneously, as seen by the disappearance of Cy3 emission (Figure 23.28, lower panel). This decay of the complex is just like the decay of an excited state, and the histogram of decay times yields the decay rate. In the case of GroEL there appears to be a time lag prior to dissociation, as seen by the rise time at short times. The authors attribute this time decay to an intermediate state of the complex that has not been identified.[55]

23.7. SINGLE-MOLECULE RESONANCE ENERGY TRANSFER

Single-molecule detection becomes an even more powerful tool when combined with resonance energy transfer (RET). Figure 23.29 shows a typical experiment in which emission spectra and lifetimes are measured for a mixture of protein molecules each labeled with a donor D. The solution also contains a fluorescent acceptor A that binds to some of the donor-labeled protein. The emission spectrum of the solution will show the presence of both the donor and acceptor. The situation is complicated because the acceptor emission will be due to two subpopulations: acceptor free in solution and acceptor bound to donor. Similarly, the donor emission spectrum will be due to two components—D and DA. Even if the intensity decays of the donor or DA pair alone are single exponentials the donor decay for the mixture would be multi-exponential because there would be two species—D and DA.

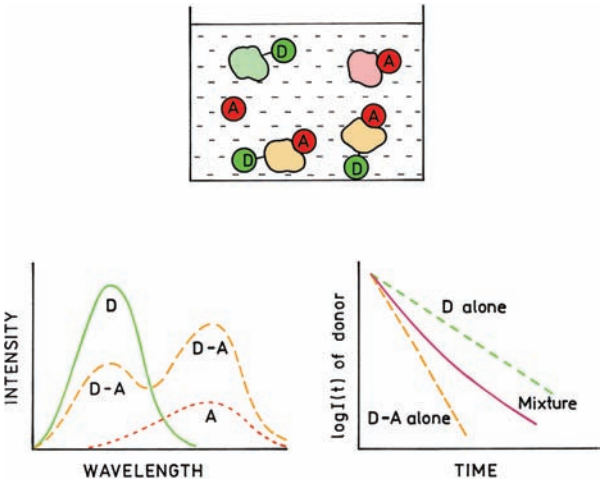

Figure 23.29. Emission spectra and intensity decay for a mixture of donor-alone (D) and donor–acceptor (D-A) pairs, and acceptor alone, as seen in an ensemble-averaged measurement.

Observations on single molecules can resolve such heterogeneity and bypass ensemble averaging. Suppose the donor-labeled protein is immobilized on a glass surface (Figure 23.30) and that single protein molecules could be separately observed. Then the signal due to any single molecule would be due to either a donor-alone molecule (left) or a protein molecule that contains bound acceptor (right).

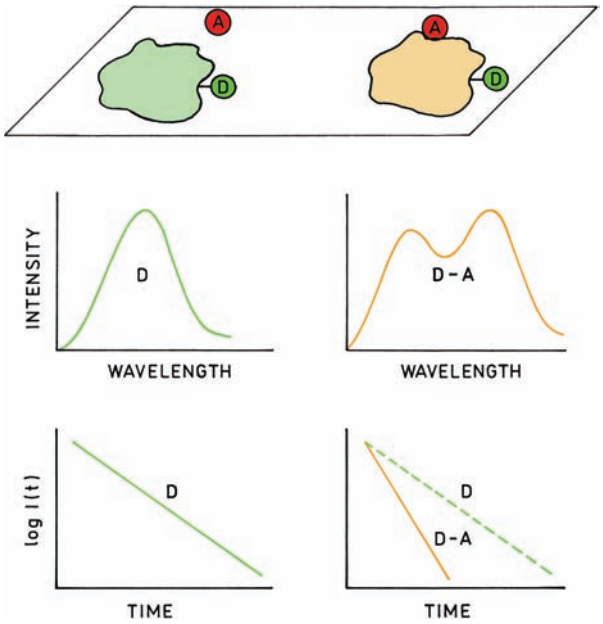

Figure 23.30. Emission spectra and intensity decays for single-molecule measurements for a mixture of donor-alone and donor–acceptor pairs immobilized on a surface.

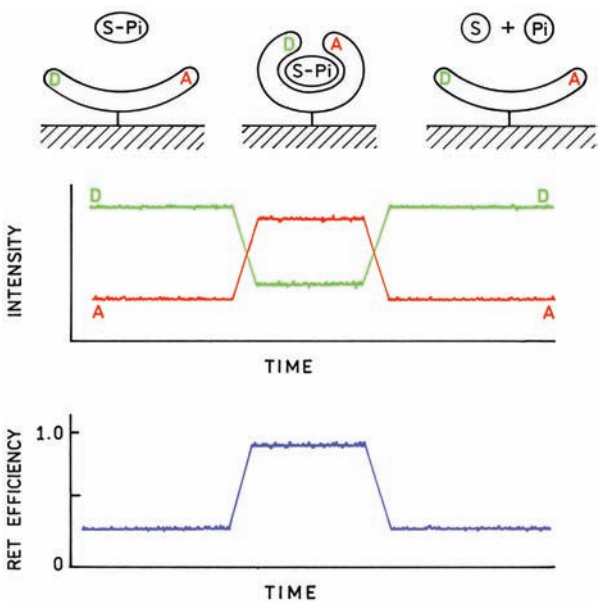

Figure 23.31. Schematic of enzyme-catalyzed hydrolysis of a substrate–phosphate (S–Pi) as seen by SMD.

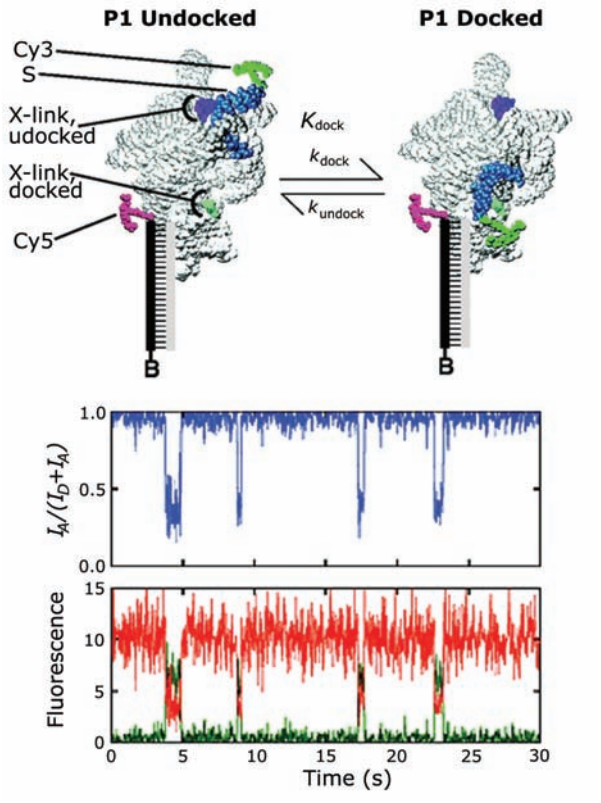

Figure 23.32. Single-molecule RET of a ribozyme molecule. The lower panels show the time-dependent donor (green) and acceptor (red) intensity and RET efficiency. Reprinted with permission from [56], [58].

As a result the emission spectrum would be that of the donor alone or of a donor–acceptor pair. Similarly, the intensity decay would be a single exponential, a longer lifetime for the donor-alone and a shorter lifetime for the DA pair. Hence observation of the single protein molecules allows the properties of each species (D and DA) to be measured.

Single-molecule RET can also be used to detect conformational changes in macromolecules. Assume the macromolecule is labeled with both a donor and an acceptor. Suppose the donor and acceptor are initially too far apart for RET but closer together when a complex is formed (Figure 23.31). Complex formation will result in a decrease in donor intensity and increased acceptor intensity. These intensity changes can be used to calculate the efficiency of energy transfer at any point in time. This coupling of changes in the donor and acceptor intensities provides a direct approach to study the dynamics of macromolecules.

Single-molecule RET has been used to follow conformational changes in a single ribozyme molecule.[56] Figure 23.32 shows a ribozyme from *Tetrahymena thermophila*. The ribozyme was linked to the surface by extending the 3' end of the ribozyme. An oligonucleotide complementary to the extension was bound to the surface by biotin–streptavidin chemistry. This tethering oligo was also labeled with a Cy5, providing the acceptor labeling on the ribozyme. The substrate of the reaction, which is another short oligonucleotide, was labeled with Cy3 as the donor. The labeled molecules were observed using TIR microscopy.

The lower panel in Figure 23.32 shows the time traces of the Cy3-donor and Cy5-acceptor emission. These signals are clearly anticorrelated, when the donor intensity drops the acceptor intensity increases, and vice versa. These signals were used to calculate the time traces for RET, showing oscillations from about 35 to 100%, indicating a change in D–A distance from about 70 to 15 Å. These data thus revealed the time-dependent motions of the labeled substrate on the ribozyme, which is shown schematically in the figure. It is clear from these examples that single-molecule studies of biomolecules can provide unique insights into the function and dynamics of biomolecules.

23.8. SINGLE-MOLECULE ORIENTATION AND ROTATIONAL MOTIONS

Since single molecules can now be detected, laboratories have started performing more detailed spectroscopic measurements.[57–60] Studies of polarized emission from single fluorophores provides some unique opportunities. At first glance the experimental results are counterintuitive when viewed from the perspective of ensemble-averaged measurements (Chapters 10–12). It is easier to understand the single-molecule results following an intuitive description of the unique features of single-molecule polarized emission. We are using both the terms polarization and anisotropy because there is presently no standardized formalism for SMD. Both the polarization and anisotropy are useful under different experimental conditions.

Figure 23.33 (top panel) shows a schematic optical configuration and results for a single fluorophore with colinear absorption (A) and emission (E) dipoles, where $\beta = 0$, and β is the angle between the transition moments. In such experiments the excitation is frequently delivered to the sample by an optical fiber. Assume there is a single immobilized fluorophore with its transition moment oriented along the x-axis, and that the emission is observed without a polarizer. Recall that the probability of absorption is proportional to $\cos^2\theta$, where θ is the angle between the absorption transition moment A and the incident electric field. As the electric vector of the incident light is varied the intensity changes as $\cos^2\theta$ (top panel). The maximum intensity occurs at $\theta = 0$, where the incident field is parallel to A.

Now consider excitation with unpolarized light (Figure 23.33, lower panel) with observation through a polarizer. Rotating the emission polarizer will yield the same result, with the intensity changing as $\cos^2\theta$. In fact, polarization of the incident light does not affect the result, except at $\theta = 90°$ when the fluorophore is not excited. The emission always displays $\cos^2\theta$ dependence centered at $\theta = 0$ because the single molecule radiates as a dipole oriented along the z-axis. Assume in the lower panel the intensity along the x-axis is $I_{\parallel}$, and $I_{\perp}$ along the y-axis. Both the polarization and anisotropy are 1.0. Recall that the highest anisotropy of a solution is 0.4, which is the result of $\cos^2\theta$ photoselection with ensemble averaging. Recall that a fluorophore always emits from the lowest singlet state. As a result the polarization of a single molecule is the same independent of the polarization of the excitation. SMD avoids averaging, returning the value of 1.0 expected for a single fluorophore (Chapter 10).

Now consider similar measurements for a fluorophore with perpendicular absorption and emission dipoles, where $\beta = 90°$ (Figure 23.34, top). Assume the angle of the incident field is rotated, and the emission is observed without an emission polarizer (top). One obtains the same $\cos^2\theta$ dependence as for $\beta = 0$. Notice the maximum is again at θ

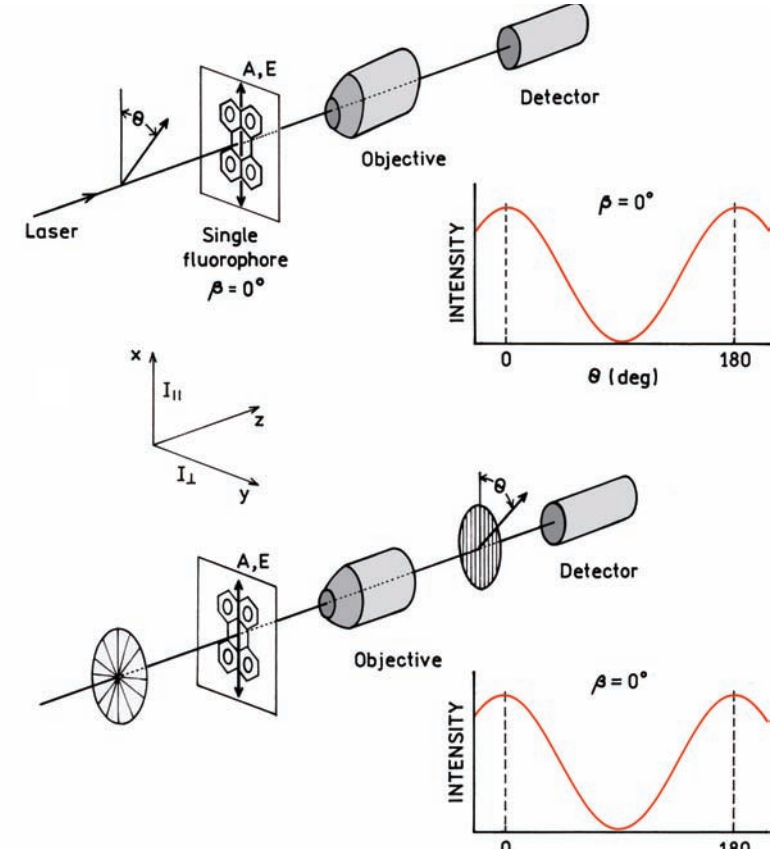

Figure 23.33. Polarization properties of a single fluorophore with colinear (β = 0) absorption (A) and emission (E) dipoles.

= 0°, even though β = 90°. This surprising result can be understood as the result of the $\cos^2\theta$ dependence on absorption. Since the fluorophore is observed without an emission polarizer the maximum signal is seen when the excitation rate is the highest, at θ = 0. A different result is obtained if the fluorophore is excited with unpolarized light and observed through an emission polarizer (Figure 23.34, bottom panel). Now the $\cos^2\theta$ dependence is shifted 90° due to θ = 90°. The same dependence on $\cos^2\theta$ would be observed for any polarization of the incident light because the emission intensity through the polarizer is determined by the position of the emission dipole. The polarization of the emission is –1.0 because the emission is polarized along the *y*-axis.

In a typical ensemble anisotropy measurement one usually rotates the emission polarizer to perform the measurement (Chapter 10). However, in Figure 23.33 and 23.34 (top panels) the excitation polarization was rotated. This is frequently done in polarized fluorescence microscopy because of the depolarizing effects of the microscope objective. If linearly polarized light is passed through the aperture and focused on the sample or molecule, the field is partially depolarized.[61] This effect is a result of the large numerical aperture and the different angles of incidence for light, passing through the center or the outer region of the objective. Light can be brought to the sample without this effect if the light is not passed through the objective, but instead directly to the sample (Figure 23.35). The larger aperture of the objective does not affect the emission measurements because the objective simply collects the emission which depends only on the orientation of the incident polarization and the fluorophore. The orientation of the incident polarization defines the parallel component ($I_{\|}$). This component can be rotated to be at any angle in the focal plane. Of course, the single molecule will only be excited if its absorption dipole has a component along the incident electric field. The emission is collected by an objective and passed through a filter to remove the scattered light.

In single-molecule experiments every photon is valuable. The molecule may display blinking and will be

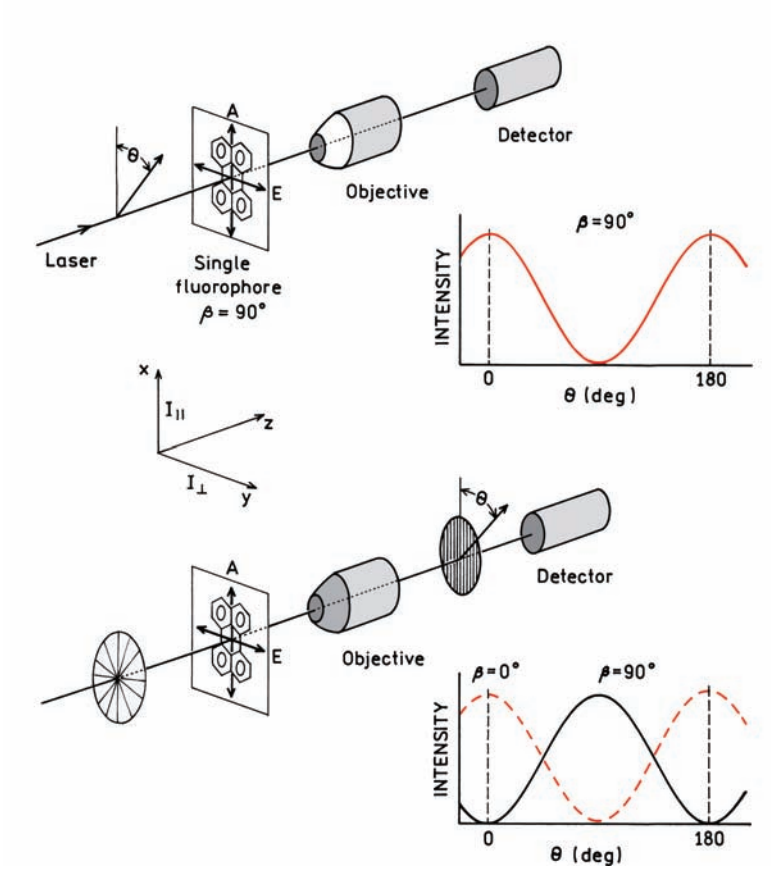

Figure 23.34. Polarization properties of a single fluorophore with perpendicular absorption (A) and emission (E) dipoles.

destroyed after a short period of observation. For these reasons it is not practical to rotate an emission polarizer to separately measure the two polarized components of the emission. These polarized components are easily separated with a polarizing beamsplitter (Figure 23.35). With this device the p-component relative to the reflective surface of the beamsplitter is p-polarized. The s-polarized component is not reflected and passes through the device.[62] See Chapter 2 for a definition of p and s polarization. One can see that the p-polarized intensity (I_P) corresponds to the parallel intensity ($I_{||}$), and the s-polarized component (I_S) corresponds to the perpendicular intensity ($I_{\perp}$). The relative detection efficiencies of the two channels (G-factor) can be measured with solution of fluorophores which displays an anisotropy of zero. It is important to remember that the objective will depolarize the emission to some extent due to its large collection angle.[61,63]

In this discussion of single-molecule polarization we assumed that the dipoles were perpendicular to the optical axis. In reality the transition moments will also have components along the optical axis that are out of the sample plane. Rather than present the somewhat complex mathematical expression to describe these cases, then intuitive concepts in Figures 23.33 and 23.34 will provide an understanding of the experimental results for singe molecules.

23.8.1. Orientation Imaging of R6G and GFP

The optical configuration shown in Figure 23.35 was used to study R6G molecules in a polymer.[64–65] A number of R6G molecules were imaged by scanning the sample stage. The images (Figure 23.36) were obtained by simultaneous measurement of the s and p components. The left and middle images show these polarized components. During the scan the signal in each image transiently disappears which looks like blinking. However, the summed image (right) does not show the dark vertical line which indicates the fluorophores are not blinking under these experimental conditions. These results indicate that the R6G molecules displayed rotational diffusion or jumps in the polymer. This is

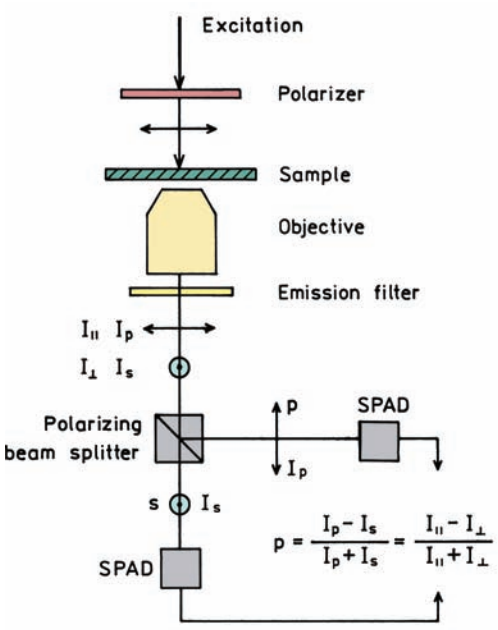

Figure 23.35. Typical configuration for single-molecule polarization measurements.

reasonable when one recalls it takes considerable time to scan the sample stage, so the molecule can rotate before the stage returns to that molecule for a second illumination.

Another approach to single-molecule orientation imaging is to use polarized excitation. As shown in Figure 23.33 the emission will show the same polarization independent of the polarization of the incident light. Polarized excitation was used with NSOM to image GFP in poly(acrylamide) (Figure 23.37). Excitation was accomplished with an aluminum-coated fiber optic with a 70-nm aperture using 488-nm laser light.[66] The relative intensities in the two polarized channels were used to calculate the orientation of the transition dipoles on the slide. Since the emission remained polarized during the scan, the GFP molecules were immobilized by the poly(acrylamide) gel. The images show that the individual GFP molecules each have different photostabilities. Molecules 2 and 3 are stable and did not blink. Molecules 4 and 5 displayed blinking. Molecule 1 appears to have been photobleached during the scan.

Single-molecule orientations can also be determined using NSOM and the shape of the single-molecule image.[67–69] Figure 23.38 shows a focused-ion-beam (FIB) image of the NSOM probe. The probe is coated with aluminum, except for the small dark ring in the center (a). The sample was $DiIC_{12}$ in PMMA. Image b shows the NSOM images when the excitation is circularly polarized. The images are not simple circles because of the sharp electric-field gradients that exist near the tip of the metal-coated fiber. Because of these field gradients the interactions of the fluorophore with the NSOM tip depend on its location and the orientation of the transition moments.

The orientation of the fluorophore can be determined from the shapes, but the theory is rather complex. The lower two images were obtained using linearly polarized light, as shown by the arrows. All the images are color coded according to the detected polarization. One of the circular images in panel b becomes a double-labeled image with linearly polarized excitation in panels c and d. These polarized NSOM images provide remarkable detail on fluorophore orientation.

23.8.2. Imaging of Dipole Radiation Patterns

Advanced Topic

The previous results on single-molecule polarization imaging were obtained using point-by-point measurements and a

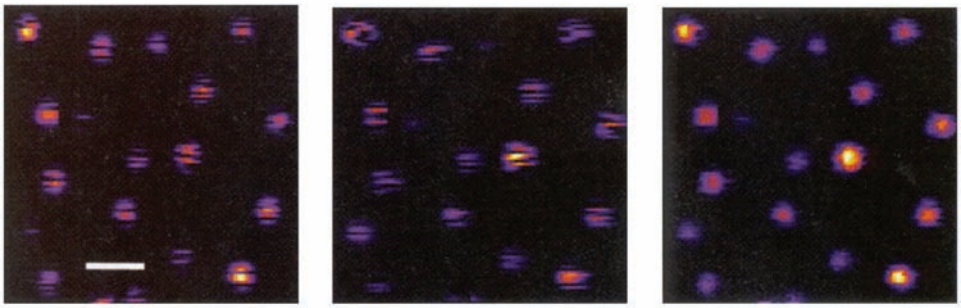

Figure 23.36. Polarized emission images of R6G molecules in poly(methylmethacrylate). The PMMA had a glass temperature of 8°C. The two orthogonal polarization images (left and center) were used to construct the summed image (right). The white bar is 1 μm. Reprinted with permission from [64].

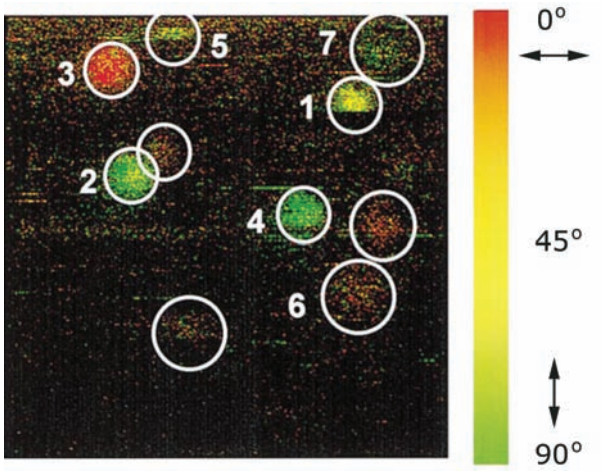

Figure 23.37. NSOM orientation imaging of GFP in poly(acrylamide). Image size 1.8 x 1.8 μm. Reprinted with permission from [66].

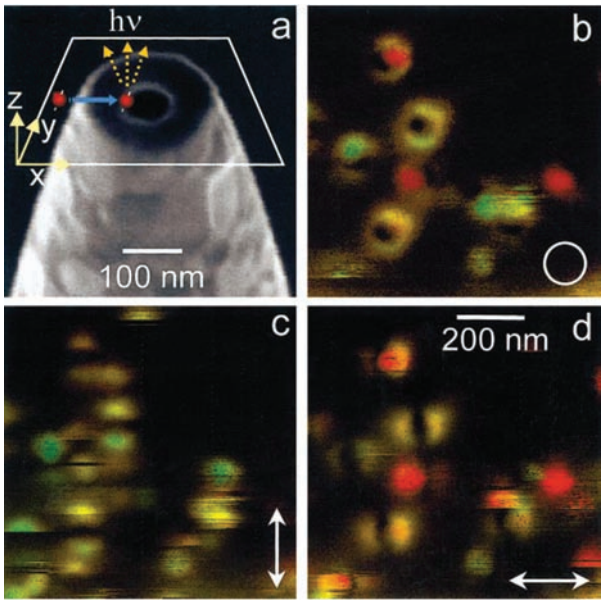

Figure 23.38. Imaging of dipole orientation using NSOM. The sample was $DiIC_{12}$ in PMMA. The circle and arrows represent the incident polarization. The green-to-red scale indicates the polarization of the emission. Reprinted with permission from [68].

scanning sample stage. It is also possible to determine fluorophore orientations by a direct imaging method.[70–74] The theory is rather complex, but the result is intuitively simple. If the light collection optics are perfect each fluorophore will appear as a diffraction limited spot, irrespective of its orientation. However, if there is a slight mismatch in the immersion fluid then light entering the objective at different

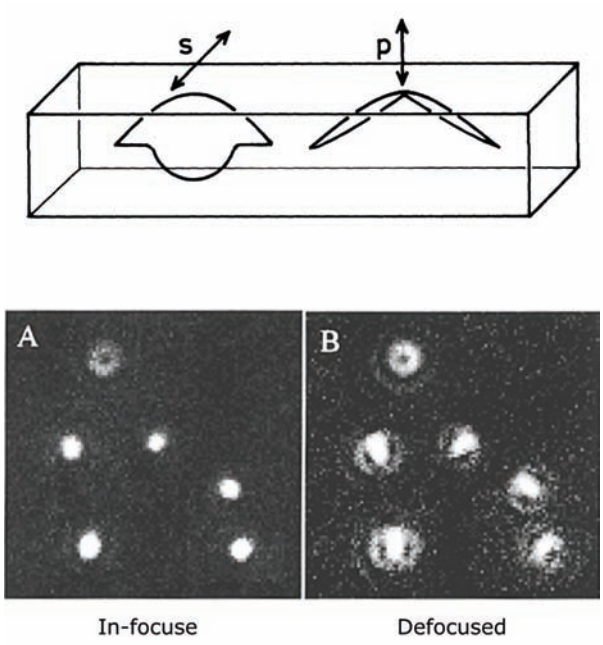

Figure 23.39. Imaging of single molecule $DiIC_{12}$ in PMMA. Upper panel shows radiation pattern for a dipole near a dielectric interface. Reprinted with permission from [70].

angles is not focused at the same point. Figure 23.39 shows such images. The spatial emission patterns are dots, circles, or a more complex distorted circle with a central dot. These images can be understood by the angle-dependent radiation patterns for a dipole near a dielectric interface (top schematic). These patterns can be calculated from classical electrodynamics. The image on the left was obtained with the fluorophores in the focal plane and the image on the right was obtained with slight defocusing. In this latter image the transition moments perpendicular to the interface (p) result in a doughnut-like image. This can be understood from the strong angular dependence of the p-dipole coupling into the glass substrate. Transition moments paralleled to the interface (s) yield filled circles. If the image is slightly defocused (right) additional information becomes available. The images become distorted along the direction of the dipole orientation. Remarkably, it is now possible to image not only single molecules, but to image their orientations as well.

23.9. TIME-RESOLVED STUDIES OF SINGLE MOLECULES

Time-resolved ensemble measurements frequently reveal multi-exponential decays for seemingly homogeneous sam-

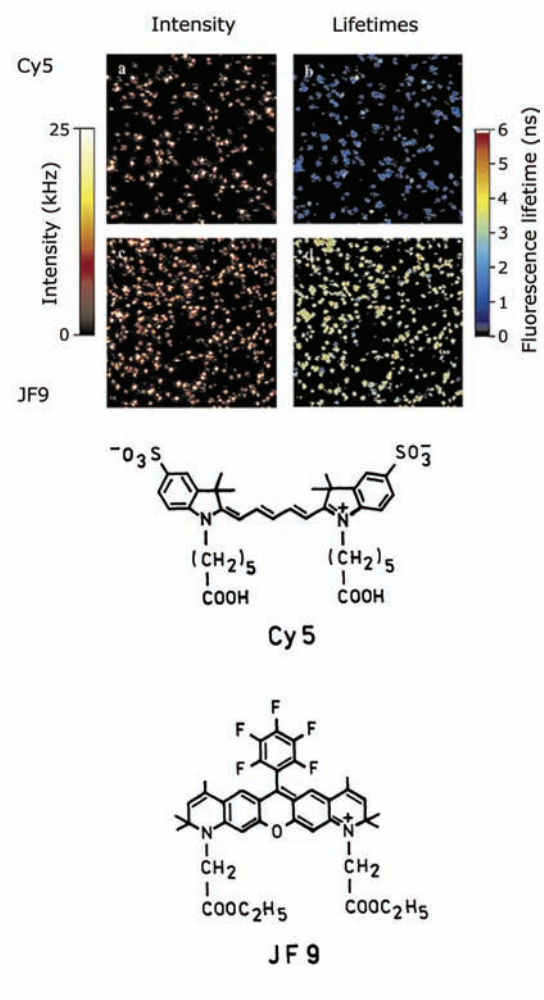

Figure 23.40. Single-molecule intensities (left) and lifetimes (right) for Cy5 (top) and JF9 (bottom) on a glass surface. Images were obtained using confocal laser scanning microscopy. The lifetimes of Cy5 and JF9 are near 2 and 4 ns, respectively. Reprinted with permission from [78].

ples, particularly for biomolecules. Such results are frequently explained as the result of some underlying heterogeneity, such as the rotamer conformations for tryptophan (Chapter 16). Hence it is natural to use time-resolved detection with single molecules to observe the properties of each subspecies. Several reports have appeared on time-resolved SMD. To date essentially all such studies have been performed using TCSPC at a defined position in the sample.[75–78] Typically the sample is raster scanned to find the locations of the molecules. The stage is then repositioned on the molecule of interest, which is excited with a pulsed laser. The repetition rate of the laser is typically 1 MHz or higher and the dwell time at each location is about 1 ms. There is time for a number of pulses to arrive at the sample during the dwell time. The time intervals between the start and stop pulses are recorded along with an identifier for the location of the molecule on the slide.

An example of single-molecule lifetime imaging is shown in Figure 23.40 for Cy5 and JF9. The two left panels are the intensity images. The dyes cannot be distinguished based on the intensities. The two right images show the lifetime for Cy5 (top) and JF9 (bottom). The two fluorophores can be distinguished from the lifetimes, even at the single-molecule level. The measurements were then extended to a mixture of Cy5 and JF9 (Figure 23.41). The two fluorophores cannot be distinguished in the intensity image (left). However, the individual fluorophores can be identified from the fluorescence lifetime (right). Since lifetimes are independent of the total intensity, and since the fluorophores photobleach, we can expect to see more uses of single-molecule lifetime imaging. These applications will be facilitated by the increasing ease of lifetime measurements using pulsed laser diodes and modern electronics.

23.10. BIOCHEMICAL APPLICATIONS

23.10.1. Turnover of Single Enzyme Molecules

Single-molecule detection has been used to image the activity of individual enzyme molecules. The protein cholesterol oxidase (Cox) was immobilized in an agarose gel.[79] Polarization studies showed that the protein displayed rotational diffusion, but the gel prevented translational diffusion. Cox catalyzes the oxidation of cholesterol, as shown in the top panel of Figure 23.42. The cofactor FAD is tightly bound to the enzyme and is not expected to dissociate. The slide containing immobilized enzyme was imaged by scanning a 442-nm HeCd laser beam across the sample. Recall that the oxidized form of FAD is fluorescent (Chapter 3). Hence the reaction results in transient emission from the FAD until it is reduced by the enzymatic reaction. The on–off fluorescence from the protein results in bright spots due to single Cox molecules (Figure 23.43). The spots display a range of intensities. This is because photon counts are accumulated for the entire time the oxidized form is present on the protein. FAD itself did not display blinking under these conditions. If a single spot is examined with higher time resolution it displays a blinking intensity, which indicates reduction or oxidation of the cofactor (Figure 23.42, lower panel). Accumulation of a longer time trace and examination of multiple enzyme molecules allowed the Michaelis-

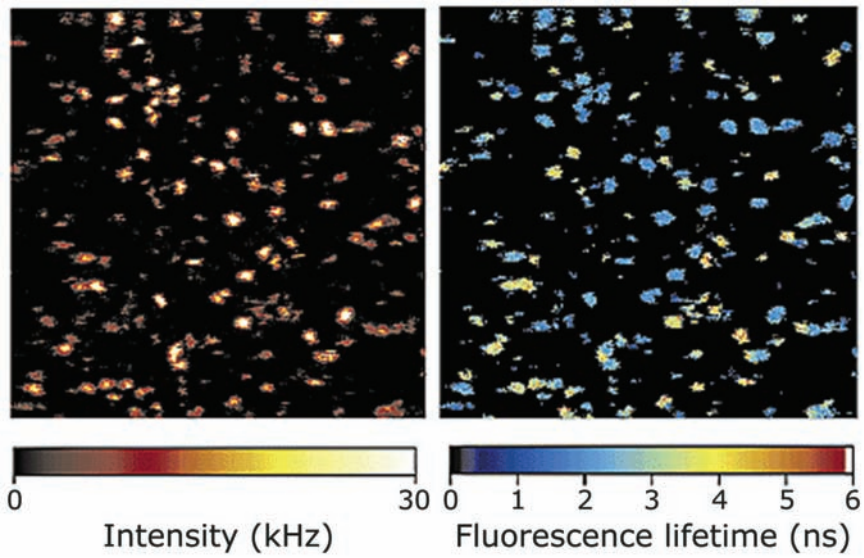

Figure 23.41. Single-molecule intensity and lifetime images for a mixture of Cy5 and JF9 on a glass surface. Reprinted with permission from [78]. Copyright © 2002, American Chemical Society.

Menten rate constants to be determined from the reaction-induced blinking.[79]

Another example of single-molecule enzyme kinetics is shown in Figure 23.44. The enzyme dihydroorotate dehydrogenase (DHOD) catalyses a reaction in the first step of de-novo pyrimidine synthesis. In this reaction cycle FMN is reduced and oxidized. Unfortunately, the flavin is quenched by a tyrosine residue in the wild-type *E. coli* protein (Figure 23.44). To obtain a useful signal the nearby tyrosine residue responsible for the quenching was mutated to a leucine.[80] The enzyme molecules were immobilized in a 1% agarose gel and localized by the flavin emission. However, the emission quickly disappeared (Figure 23.45), and the disappearing signal was due to dissociation of FMN from the protein and not photobleaching. Because the rate of disappearance was not dependent on incident power, in the presence of substrates the FMN displayed rapid blinking in addition to disappearance that was the result of the oxidation–reduction cycles occurring prior to dissociation (Figure 23.45). The distribution of on and off times could be used to determine kinetic constants for the reaction.

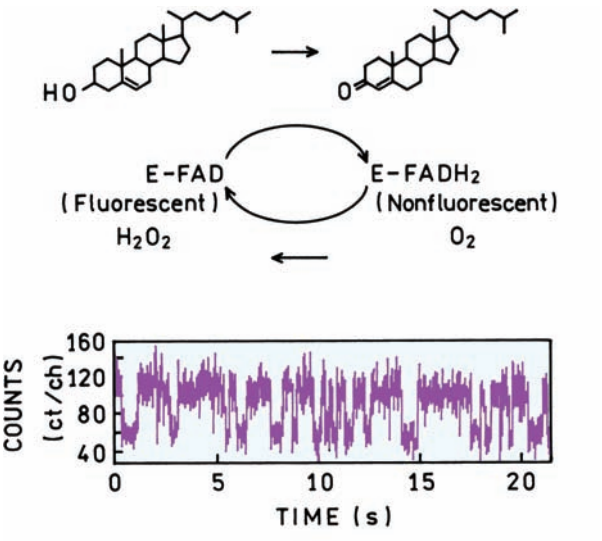

Figure 23.42. Blinking of FAD emission during oxidation of cholesterol by Cox. The top panel shows the chemical reaction. Revised from [79].

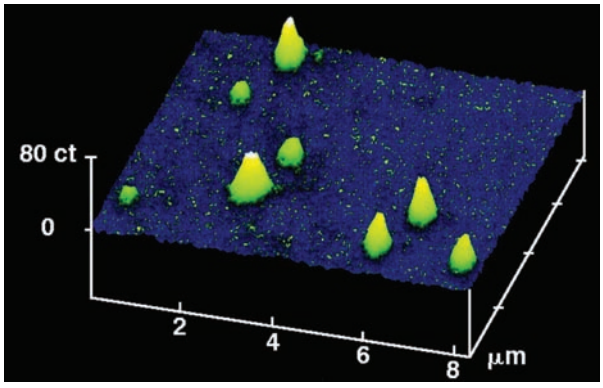

Figure 23.43. Single-molecule images of cholesterol oxidase as seen from the emission of FAD. Reprinted from [79].

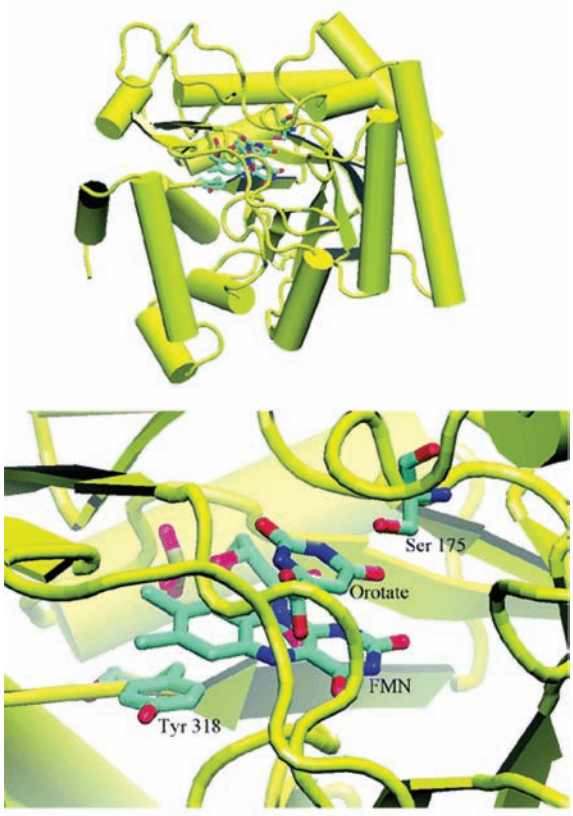

Figure 23.44. **Top**: Structure of wild-type DHOD from *E. coli*. **Bottom**: Environment of FMN in the catalytic site. Reprinted with permission from [80]. Copyright © 2004, American Chemical Society.

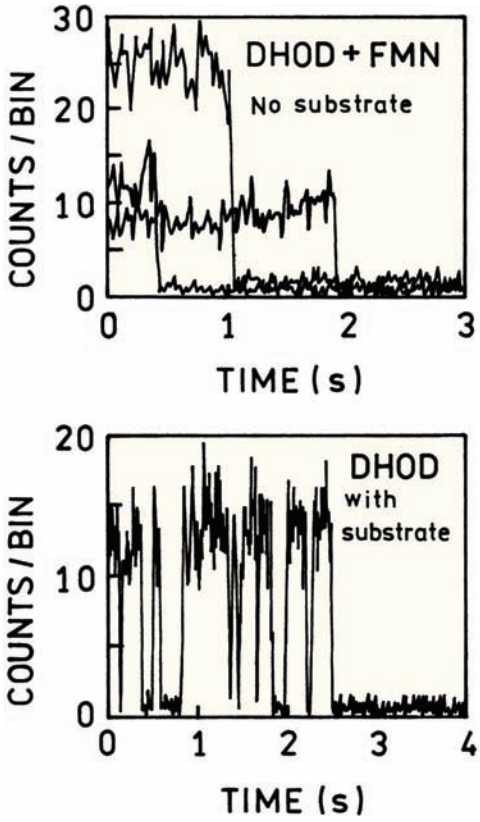

Figure 23.45. Emission intensities of FMN bound to dihydroorotate dehydrogenase in the absence (top) and presence (bottom) of substrates. The top panel shows traces for three different molecules. The protein was immobilized in an agarose gel. Reprinted with permission from [80]. Copyright © 2004, American Chemical Society.

23.10.2. Single-Molecule Molecular Beacons

We started this chapter with a schematic of a single-molecule molecular beacon (Figure 23.1). In fact, such an experiment has been reported.[81] Figure 23.46 shows a surface-bound molecular beacon. This sequence has a biotin on one end and the fluorophore MR121 at the opposite end. The sequence is designed so that a guanine residue is next to MR121 when the beacon is in the hairpin conformation. In solution this beacon displays a sixfold increase in intensity when hybridized with the complementary oligo.

The lower panels in Figure 23.46 show confocal images of surface-bound beacons in the absence (left) and presence (right) of the complementary oligo. Hybridization with the complementary oligo results in an increase in the number of observable spots. The actual increase in intensity is larger than it appears because the scale on the left image is four times smaller than the right image. This approach allows detection of single hybridization events.

23.10.3. Conformational Dynamics of a Holliday Junction

Single-molecule FRET has been extensively useful in studies of the conformational dynamics of DNA and RNA.[82–88] One example is a study of the structural dynamics of a Holliday junction.[83] Genetic recombination is an important component of genetic diversity and evolution. Recombination occurs when sections of DNA are exchanged between chromosomes. This recombination occurs at sites that are called Holliday junctions. These junctions or sections of DNA form a four-way cross (Figure 23.47). These junctions are formed and break when DNA strands are exchanged.

The Holliday junction in Figure 24.47 contains four DNA oligomers. One oligomer was synthesized with a donor (Cy3) and a second oligomer was synthesized with an acceptor (Cy5) both on the 5' ends of the DNA strands. A third strand was labeled with biotin for surface immobilization. The four-way junction was expected to change its con-

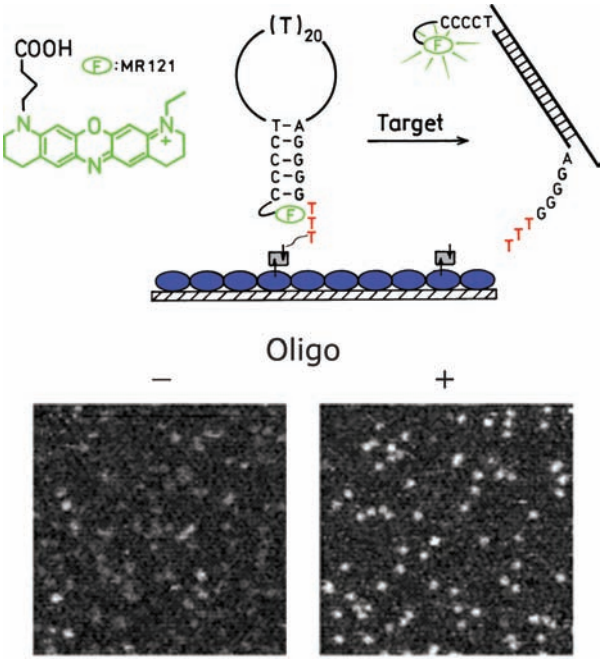

Figure 23.46. Confocal images of an immobilized beacon, with and without the complementary oligo, respectively. The left and right intensity scales are 0–4 and 0–16, respectively. Reprinted with permission from [81]. Copyright © 2003, American Chemical Society.

formation to position the Cy3 and Cy5 close to each other, or more distant, resulting in changes in energy transfer.

Figure 23.48 shows the single-molecule time traces of two different junctions, each with a different sequence. In both junctions the donor and acceptor intensities fluctuate. The intensity changes are anticorrelated, showing that the fluctuations are due to energy transfer between Cy3 and Cy5. In single-molecule studies the extent of energy transfer is presented as $E_{FRET} = I_A/(I_A + I_D)$, rather than an actual transfer efficiency. The extent of energy transfer fluctuates between two levels. This indicates that there is no significant population of the intermediate state shown in the center of Figure 23.47. These junctions exist in only two conformations. The single-molecule RET data also show that the sequence affects the preferred conformation. Junction 3 remains mostly in the form with high-energy transfer. Junction 7 is equally distributed between the two states (Figure 23.48).

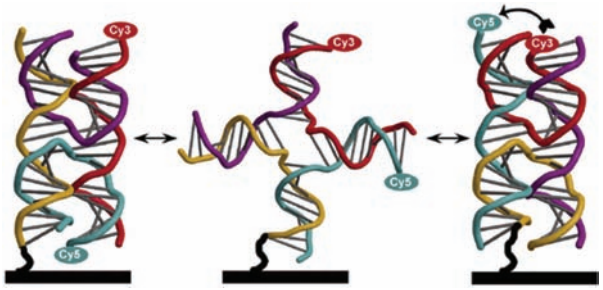

Figure 23.47. Structural flexibility in a DNA four-way Holliday junction. Reproduced with permission from [82]. Copyright © 2003, American Chemical Society.

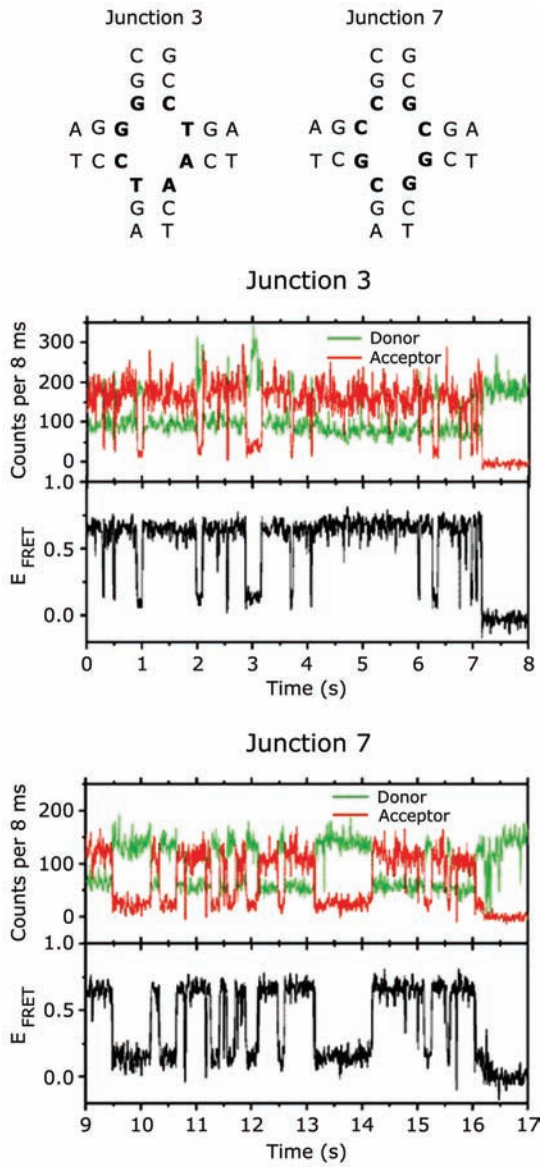

Figure 23.48. Single-molecule conformational changes in two Holliday junctions. Junctions 3 and 7 refer to different sequences; $E_{FRET} = I_A/(I_A + I_D)$. Reprinted with permission from [83].

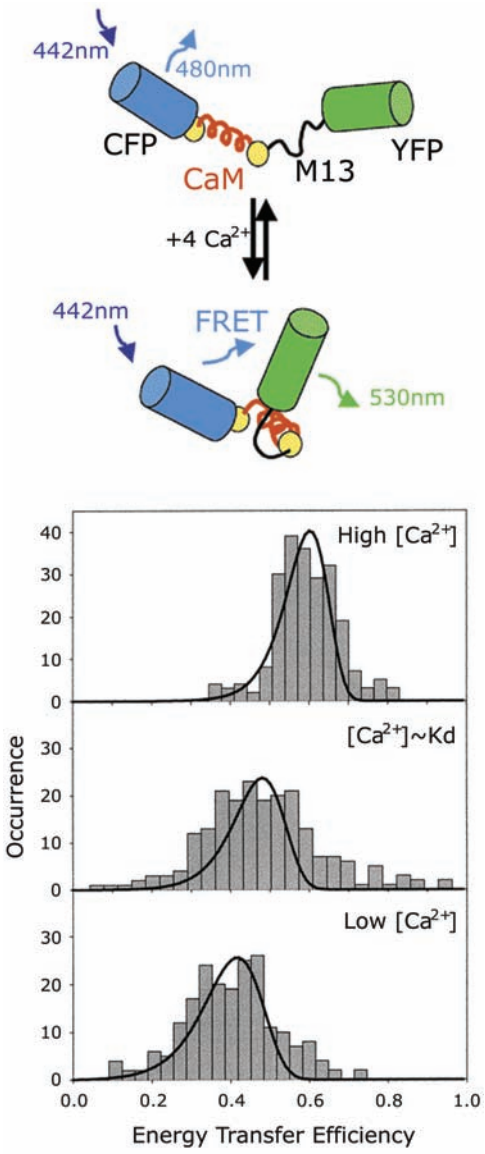

Figure 23.49. Calcium sensor based on a GFP donor–acceptor pair linked by calmodulin (CaM) and the M13 peptide. The panels show the single-molecule RET efficiency. Reprinted with permission from [10, 89].

23.10.4. Single-Molecule Calcium Sensor

Single-molecule detection has been extended to single-molecule sensors.[89] A single-molecule sensor was designed according using two GFPs as a donor–acceptor pair, linked by calcium-sensitive proteins (Figure 23.49). The linker consisted of calmodulin (CaM) and the M13 peptide. In the presence of calcium CaM expresses a hydrophobic region that binds the M13 peptide, bringing the GFPs closer together.[90] Single molecules of a similar sensor were observed using a confocal scanning microscope. The individual molecules were examined at various concentrations of calcium. Histograms were constructed showing the number of times a particular transfer efficiency was observed. These histograms show the closer average distance of the donor and acceptor in the presence of calcium. In this case the distributions are rather wide, with overlap of the high- and low-calcium histograms. This suggests that this sensor adopts more than two conformations in the presence of calcium.

23.10.5. Motions of Molecular Motors

Motion occurs constantly in cells and tissues, and are due to a variety of proteins. Intracellular transport of organelles, mRNA, and other molecules is due in part to kinesin. Kinesin is a dimeric protein that moves along actin filaments while it consumes ATP. Single-molecule imaging has been used to follow the motion of kinesin[91] and other proteins.[92–95] For kinesin there were two possible modes of motion: hand-over-hand and inchworm motion (Figure 23.50). Previous studies had shown that the central stalk in kinesin does not rotate during motion, so this mechanism was not considered.

To study kinesin motions one of the actin-binding domains was labeled with Cy3 and the other left unlabeled.[91] Actin filaments were immobilized on the slides to provide a binding site for kinesin. Upon addition of ATP the Cy3 spot was found to move in discrete steps (Figure 23.50, lower panel). Several different kinesin mutants were labeled and studied, and all displayed similar step sizes. The size of the steps allowed selection of the hand-over-hand model for kinesin motion. The average step size of 17 nm was consistent with the size of two actin molecules. The inchworm mode of motion would have resulted in a smaller 8.3-nm step size.

23.11. ADVANCED TOPICS IN SMD

23.11.1. Signal-to-Noise Ratio in Single-Molecule Detection

We have now seen examples of SMD. These experiments all had one feature in common, which is careful design of the sample and optical system to achieve an adequate S/N ratio. In order to detect a single molecule the signal from the molecule must be larger than the fluctuations in the background signal. Additionally, all single-molecule exper-

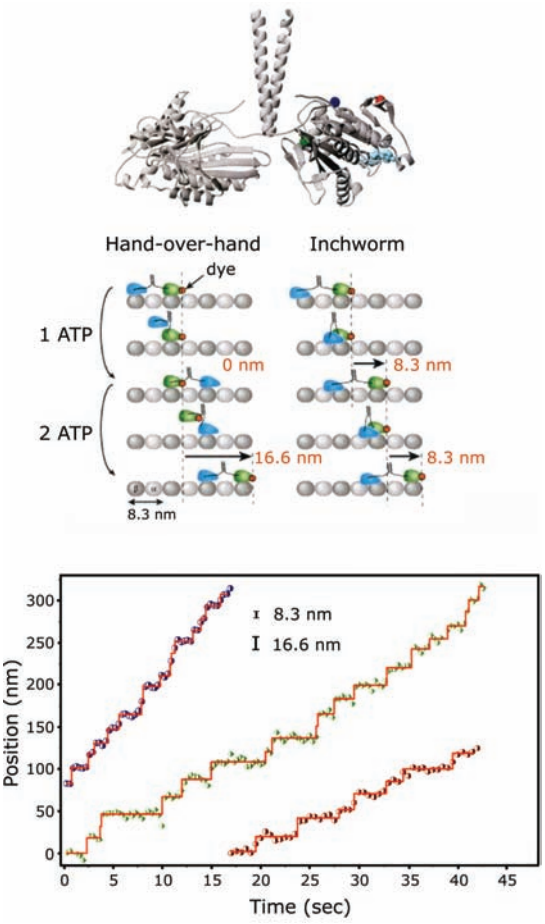

Figure 23.50. Possible mechanisms for movement of kinesin on actin filaments. The lower panel shows the time-dependent motion and the distance for each step. Reprinted with permission from [91]. Copyright © 2000, American Chemical Society.

iments are performed over a limited range of incident intensities, concentrations, and dye characteristics. At present it is only possible to observe single molecules above the background under certain conditions. For SMD the S/N ratio is given by[16]

$$S/N = \frac{DQ\left(\frac{\sigma}{A}\right)\left(\frac{P_0}{h\nu}\right)T}{\sqrt{\left(\frac{DQ\sigma_P P_0 T}{Ah\nu}\right) + C_B P_0 T + N_D T}} \qquad (23.6)$$

In this expression D is the instrument detection efficiency, Q is the quantum yield of the fluorophore, σ is its absorption cross-section, A is the illuminated area, $P_0/h\nu$ is the number of incident photons per second, and T is the data collection time. In the denominator C_B is the number of background counts per watt of incident power and N_D the number of dark counts per second. At first glance this expression appears complex but its meaning becomes clear upon examination. The term in the numerator represents the signal from the fluorophore. The three terms in the denominator are the signals from the fluorophore, autofluorescence from the sample and instrument, and the number of dark counts recorded by the detector. The denominator is raised to one-half power because it represents the fluctuations or noise in the intensity rather than the intensity itself.

Figure 23.51 shows calculations of the S/N ratio for assumed parameter values that roughly describe R6G in water. The surfaces show the dependence of S/N on the incident power and observed area. The middle panel assumes there is no photobleaching, and the lower panel assumes a photobleaching quantum yield of 10^{-5}. This sur-

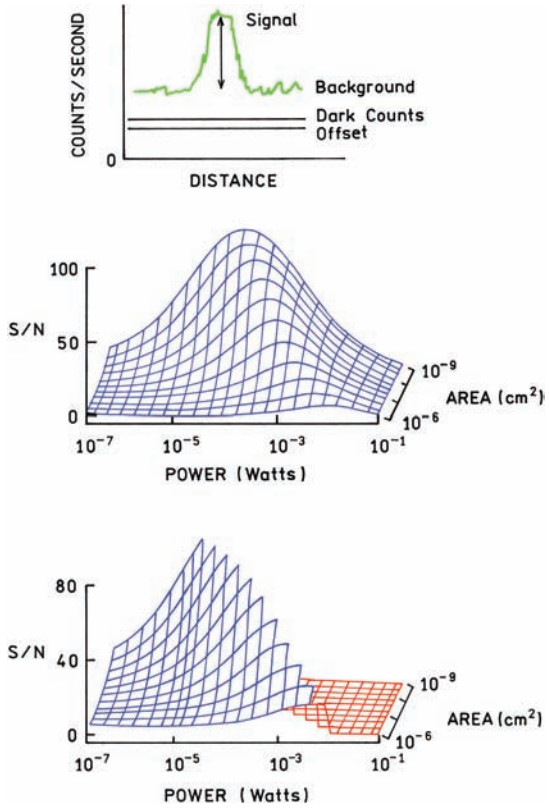

Figure 23.51. Calculations of the signal-to-noise (S/N) ratio in single-molecule detection using eq. 23.6; 532 nm, 5.6 x 10^3 W/cm^2, $Q = 0.28$, $\sigma = 4 \times 10^{-16}$ cm^2, $D = 0.072$, $N_D = 100$ cts/s, $C_B = 2 \times 10^8$ counts/W. $T = 0.1$ s. For the lower panel the photobleaching quantum yield was taken as 10^{-5}. Revised and reprinted with permission from [16], Copyright © 2003, American Institute of Physics.

face shows that even under good conditions S/N is unlikely to exceed 100. Also, S/N is adequate over a limited range of incident intensities and sample sizes. S/N initially increases with incident power, but decreases at higher power due to increased contributions from the background. The useful range of conditions is even more limited if photobleaching is considered (lower panel) because the fluorophore disappears after emitting some average number of photons. The surfaces in Figure 23.51 shows that SMD is possible because of several favorable conditions, including high photon detection efficiency, high photostability, and low dark counts. An unfavorable change in any of these parameters can make it impossible to detect the emission from a single fluorophore.

23.11.2. Polarization of Single Immobilized Fluorophores

In Figures 23.33 and 23.34 we described the polarization of single molecules when excited with polarized light. These concepts are clarified by a mathematical description of this system. Consider a fluorophore on a glass slide, with colinear absorption and emission dipoles (Figure 23.52). The transition moment is oriented at an angle θ from the *x*-axis and an angle ϕ from the optical *z*-axis. The polarized components of the emission are separated with a polarizing beamsplitter. The intensity of each polarized component is given by the square of the electric field projected onto the axis. Hence,

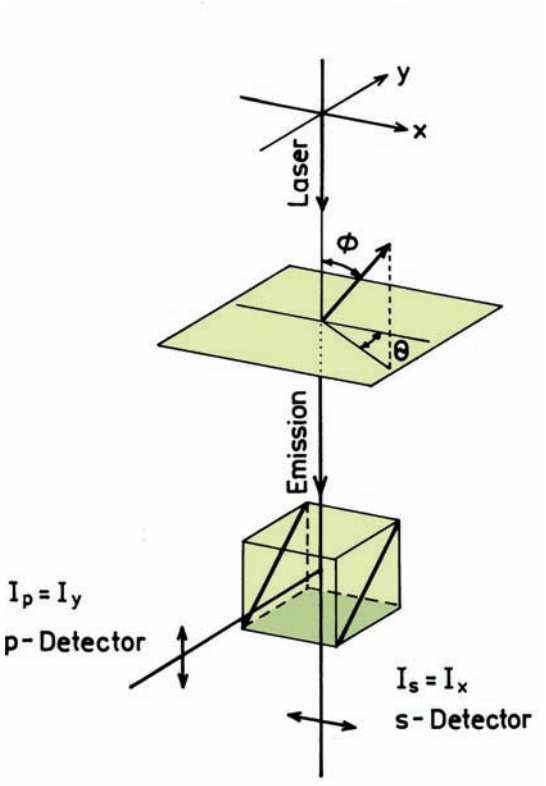

Figure 23.52. Polarized intensities for a single immobilized fluorophore.

$$I_s = I_x = k \sin^2\phi \cos^2\theta \tag{23.7}$$

$$I_p = I_y = k \sin^2\phi \sin^2\theta \tag{23.8}$$

where k is an instrument constant assumed to be the same for both channels. Notice that it was not necessary to consider the polarization of the incident light. The intensity a fluorophore emits along the *x*- and *y*-axes depends only on the orientation of the emission dipole, regardless of how the molecule was excited. The polarization of the emission is given by

$$P = \frac{I_p - I_s}{I_p + I_s} = 1 - 2\cos^2\theta \tag{23.9}$$

Perhaps surprisingly, the polarization does not depend on the angle ϕ because the intensity is proportional to the same factor $\sin^2\phi$ in both channels.

23.11.3. Polarization Measurements and Mobility of Surface-Bound Fluorophores

The ability to measure the polarization of single molecules makes it possible to measure their mobility. Because only a limited number of photons per fluorophore can be detected it may be difficult to determine the correlation time from the polarized intensity decays. An alternative approach to mobility measurements is to measure the polarized emission interaction when the excitation polarization is rotated.[96] Figure 23.53 shows such measurements of Texas Red using an electrooptic device to repetitively rotate the excitation polarization. The intensity of this single Texas Red molecule changes from nearly zero to a maximum value with rotation of the polarization. The insert shows the averaged intensities at various angles of incident polarization. There is an angle near 60° where the intensity is near zero. Recall that excitation of a single molecule is proportional to $\cos^2\theta$, so that the intensity minimum occurs where the absorption transition is perpendicular to the excitation polarization. Such a high contrast ratio is not seen for

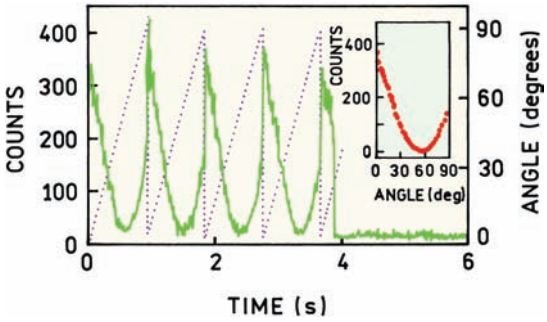

Figure 23.53. Single-molecule emission intensity of Texas Red on glass using a confocal microscope. The excitation polarization was rotated as shown. The insert shows the intensity for different excitation polarizing angles, averaged from the first four cycles. Reprinted with permission from [96].

ensemble measurements in random media because some of the fluorophores are always aligned with the incident polarization.

Single-molecule polarization measurements can provide a direct measurement of the angle between the absorption and emission dipoles.[58] Figure 23.54 shows the intensities of an immobilized Cy5 molecule. For rotation of the excitation or emission polarizer. As described in Figure 23.33 and 23.34, the angle-dependent intensities will overlap for parallel transitions and be shifted when the absorption and emission dipoles are displaced by an angle β. In the case of Cy5 the angle-dependent intensities nearly overlap. The small offset is consistent with a small angle of $\beta = 5^\circ$.

The concepts shown in Figures 23.53 and 23.54 were applied to a labeled DNA oligomer that was bound to APS-treated glass.[97] The sample was immersed in water to allow the possibility of probe rotation, but the oligomers did not migrate on the slide. The intensities of the polarized components of a single molecule were excited with different polarizations (Figure 23.55). The polarized components are completely out of phase. This is because when the fluorophore is parallel to one detection channel it is perpendicular to the other detection channel. Additionally, the correlation time of the probe must be much longer than the excited-state lifetime. Otherwise the emission in both channels would be the same. Using these considerations, molecules a, b, and e in Figure 23.55 are mobile. Molecule c must be immobilized because the intensities are in phase. The pattern seen for molecule d is characteristic of hindered rotational motion.

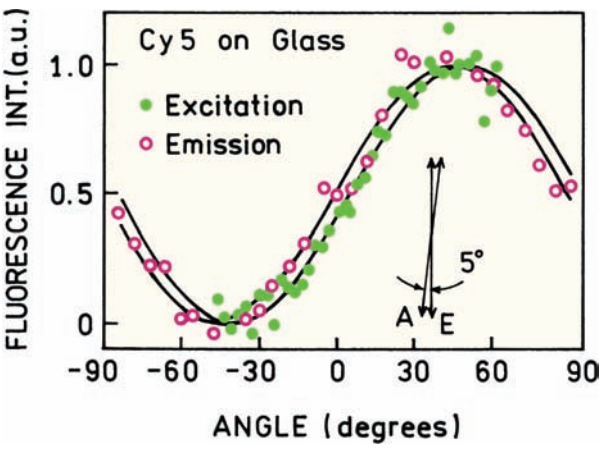

Figure 23.54. Dependence of the emission intensity of an immobilized Cy5 molecule on the angle of the excitation (●) and emission (○) polarization. The data represent an average from 15 molecules. Reprinted with permission from [58].

23.11.4. Single-Molecule Lifetime Estimation

Calculation of the lifetimes using single-molecule data requires a different algorithm from that described for

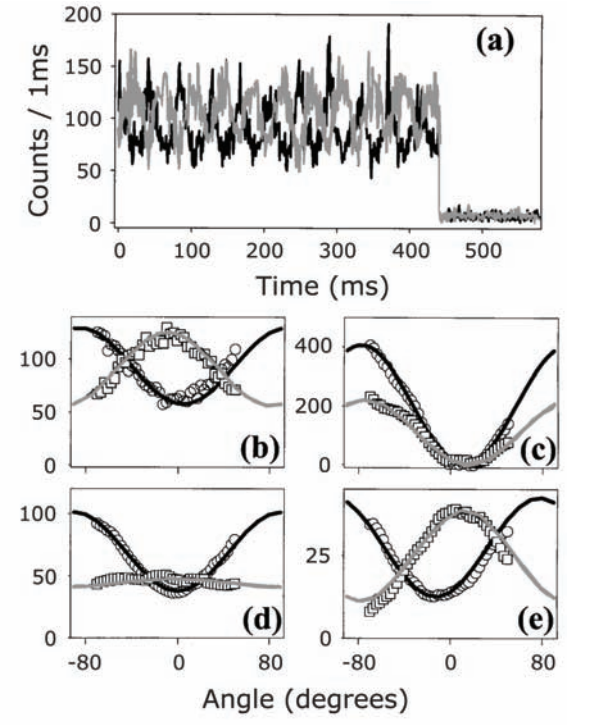

Figure 23.55. Time traces of the polarized intensities of a single labeled DNA oligomer bound to APS-treated glass. In a, b, and e the fluorophore is freely rotating. In c the fluorophore is immobile. The data in panel b are for the same molecule observed for panel a. The pattern in panel d is said to be characteristic of a hindered motion. Reprinted with permission from [97].

TCSPC. For TCSPC there is usually a large number of photons in each time interval, and the measurements are accurately described as Gaussian distributions around the true value. It should be remembered that the use of nonlinear least squares is based on the assumption that measurements have Gaussian properties. For the single-molecule data there is usually a small number of counts in each time interval. As a result the number of counts in each bin is distributed according to Poisson probability function. Nonlinear least squares is not the correct approach for such data.[98]

Methods have been developed to recover single-molecule lifetimes from sparse data.[99–100] In many single-molecule experiments the goal is not to resolve multi-exponential decays, but rather to obtain the best estimate of the decay time, the decay time which has the maximum likelihood of being the correct value. For this simple case there is an analytical expression for the estimated lifetime.[100] Assume the time width of each bin is Δt and that there are m bins, so the total time width of the data is $m\Delta t = T$. Then the lifetime can be found from

$$A - B = \frac{1}{N}\sum_{i=1}^{m} i\Delta t\frac{N_i}{N} \tag{23.10}$$

where N_i is the number of counts in the ith bin and N is the total number of counts. The best estimate lifetime can be found using

$$A = \Delta t/\left[1 - \exp(-\Delta t/\tau)\right] \tag{23.11}$$

$$B = T/\left[\exp(T/\tau) - 1\right] \tag{23.12}$$

These expressions are solved interactively to recover the lifetime τ. Different expressions are needed to estimate multiple parameters by the maximum-likelihood method. The important point is that nonlinear least squares should not be used with sparse data.

23.12. ADDITIONAL LITERATURE ON SMD

The technology and applications for SMD have expanded dramatically during the past several years. It was not practical in this chapter to describe the many elegant results published on SMD. To assist the reader in finding reports of interest we have included, after the main references, a compilation of additional references on single-molecule detection that summarizes many of these reports according to their main emphasis.

In closing, SMD is a powerful technology that bypasses ensemble averaging and provides direct information on the behavior and/or kinetics of single molecules. While many papers have been published, the majority are still proof-of-principle experiments that are always necessary to systematize a new technology. The reader may notice the absence of examples on single-molecule diffusion or intracellular single-molecule detection. Several reports on these topics have appeared but were not selected as teaching examples because the results are not as clear as those shown above. It appears likely that there will be considerable difficulty performing SMD experiments on freely diffusing or intracellular species.

REFERENCES

1. Shera EB, Seitzinger NK, Davis LM, Keller RA, Soper SA. 1990. Detection of single fluorescent molecules. *Chem Phys Lett* **174**(6): 553-557.
2. Hirschfeld T. 1976. Optical microscopic observation of single small molecules. *Appl Opt* **15**(12):2965–2966.
3. Nguyen DC, Keller RA, Jett JH, Martin JC. 1987. Detection of single molecules of phycoerythrin in hydrodynamically focused flows by laser-induced fluorescence. *Anal Chem* **59**:2158–2161.
4. Peck K, Stryer L, Glazer AN, Mathies RA. 1989. Single-molecule fluorescence detection: autocorrelation criterion and experimental realization with phycoerythrin. *Proc Natl Acad Sci USA* **89**:4087–4091.
5. Moerner WE, Kador L. 1989. Optical detection and spectroscopy of single molecules in a solid. *Phys Rev Lett* **62**(21):2535–2538.
6. Bergquist JC, Hulet RG, Itano WM, Wineland DJ. 1986. Observation of quantum jumps in a single atom. *Phys Rev Lett* **57**(14):1699–1702.
7. Diedrich F, Walther H. 1987. Nonclassical radiation of a single stored ion. *Phys Rev Lett* **58**(3):203–206.
8. Jett JH, Keller RA, Martin JC, Marrone BL, Moyzis RK, Ratliff RL, Seitzinger NK, Shera EB, Stewart CC. 1989. High-speed DNA sequencing: an approach based upon fluorescence detection of single molecules. *J Biomol Struct Dyn* **7**(2):301–309.
9. Werner JH, Cai H, Jett JJ, Reha-Krantz L, Keller RA, Goodwin PM. 2003. Progress towards single-molecule DNA sequencing: a one color demonstration. *J Biotechnol* **102**:1–14.
10. Moerner WE. 2002. A dozen years of single-molecule spectroscopy in physics, chemistry, and biophysics. *J Phys Chem B* **106**:910–927.
11. Erdmann R, Enderlein J, Seidel C, eds. 1999. Single molecule detection and ultrasensitive analysis in the life sciences. *Cytometry* **36**(3):161–264.
12. Weiss S 1999. Fluorescence spectroscopy of single biomolecules. *Science* **283**:1676–1683.
13. Moerner WE, Orrit M. 1999. Illuminating single molecules in condensed matter. *Science* **283**:1670–1676.

14. Tamarat PH, Maali A, Lounis B, Orrit M 2000. Ten years of single-molecule spectroscopy. *J Phys Chem A* **104**(1):1–16.
15. Ambrose WP, Goodwin PM, Jett JH, Orden AV, Werner JH, Keller RA. 1999. Single molecule fluorescence spectroscopy at ambient temperature. *Chem Rev*, **99**(10):2929–2956.
16. Moerner WE, Fromm DP. 2003. Methods of single-molecule fluorescence spectroscopy and microscopy. *Rev Sci Instrum* **74**(8):3597–3619.
17. García-Parajó M, Veerman J-A, Bouwhuis R, Vallée M, van Hulst NF. 2001. Optical probing of single fluorescent molecules and proteins. *Chem Phys Chem* **2**:347–360.
18. Zander C, Enderlein J, Keller RA, eds. 2002. *Single molecule detection in solution: methods and applications*. Wiley-VCH, Darmstadt, Germany.
19. Enderlein J, Zander C. 2002. Theoretical foundations of single molecule detection in solution. In *Single molecule detection in solution: methods and applications*, pp. 288–324. Ed Ch Zander, J Enderlein, RA Keller. Wiley-VCH, Darmstadt, Germany.
20. Born M, Wolf E. 2002. *Principles of optics: electromagnetic theory of propagation, interference and diffraction of light*. Cambridge UP, Cambridge.
21. Halliday D, Resnick R, Krane KS. 1992. *Physics*, Vol. 2, 4th ed. John Wiley & Sons, New York.
22. Axelrod D, Hellen EH, Fulbright RM. 1992. Total internal reflection fluorescence. In *Topics in fluorescence spectroscopy*, Vol. 3: *Probe design and chemical sensing*, pp. 289–343. Ed JR Lakowicz. Plenum Press, New York.
23. Axelrod D. 1989. Total internal reflection fluorescence microscopy. *Methods Cell Biol* **30**:245–270.
24. Wilson T, ed. 1990. *Confocal microscopy*. Academic Press, New York.
25. Inoué S. 1995. Foundations of confocal scanned imaging in light microscopy. In *Handbook of biological confocal microscopy*, pp. 1–17. Ed JB Pawley (Ed.). Plenum Press, New York.
26. Lemasters JJ, Chacon E, Zahrebelski G, Reece JR, Nieminen AL. 1993. Laser scanning confocal microscopy of living cells. In *Optical microscopy: emerging methods and applications*, pp. 339–354. Ed G Herman, JJ Lemasters. Academic Press, New York.
27. Webb WW, Wells KS, Sandison DR, Strickler J. 1990. Criteria for quantitative dynamical confocal fluorescence imaging. In *Optical microscopy for biology*, pp. 73–108. Ed B Herman, K Jacobson. Wiley-Liss, New York.
28. Ambrose WP, Goodwin PM, Nolan JP. 1999. Single-molecule detection with total internal reflection excitement: comparing signal-to-background and total signals in different geometries. *Cytometry* **36**: 224–231.
29. Pawley JB, ed. 1995. *Handbook of biological confocal microscopy*. Plenum Press, New York.
30. Matsumoto B, ed. 1993. *Methods in cell biology: cell biological applications of confocal microscopy*. Academic Press, New York.
31. Diaspro A, ed. 2002. *Confocal and two-photon microscopy foundations: applications, and advances*. Wiley-Liss, New York, 56.
32. Moerner WE, Peterman EJG, Braaselet S, Kummer S, Dickson RM. 1999. Optical methods for exploring dynamics of single copies of green fluorescent protein. *Cytometry* **36**:232–238.
33. Shubeita GT, Sekatskii SK, Dietler G, Letokhov VS. 2002. Local fluorescent probes for the fluorescence resonance energy transfer scanning near-field optical microscopy. *Appl Phys Lett* **80**(15): 2625–2627.
34. Muramatsu H, Kim JM, Sugiyama S, Ohtani T. 2003. Simultaneous multicolor fluorescence imaging by scanning near-field optical/atomic force microscopy. *Rev Sci Instrum* **74**(1):100–103.
35. Vickery SA, Dunn RC. 1999. Scanning near-field fluorescence resonance energy transfer microscopy. *Biophys J* **76**:1812–1818.
36. Schmidt TH, Schutz GJ, Baumgartner W, Gruber HJ, Schindler H. 1995. Characterization of photophysics and mobility of single molecules in fluid lipid membrane. *J Phys Chem* **99**:17662–17668.
37. Weston KD, Buratto SK. 1998. Millisecond intensity fluctuations of single molecules at room temperature. *J Phys Chem A* **102**(21): 3635–3638.
38. Weber MA, Stracke F, Meixner AJ. 1999. Dynamics of single dye molecules observed by confocal imaging and spectroscopy. *Cytometry* **36**:217–223.
39. www.perkinelmer.com/optoelectronics.
40. Christenson M. 2000. Advances in detector systems for imaging single molecule fluorescence. *Single Mol* **1**(2):177–179.
41. Edmund Optics Catalogue. 2004. (See p. 79.)
42. Kaiser Optical Systems, Ann Arbor, Michigan.
43. Weston KD, Carson PJ, Metiu H, Buratto SK. 1998. Room-temperature fluorescence characteristics of single dye molecules adsorbed on a glass surface. *J Chem Phys* **109**(17):7474–7485.
44. Garcia-Parajo MF, Veerman JA, van Noort SJT, de Grooth BG, Greve J, van Hulst NF. 1998. Near-field optical microscopy for DNA studies at the single molecular level. *Bioimaging* **6**:43–53.
45. Bian RX, Dunn RC, Xie XS. 1995. Single molecule emission characteristics in near-field microscopy. *Phys Rev Lett* **75**(26): 4772–4775.
46. Chang R, Wei PK, Fann WS, Hayashi MT, Lin SH. 1997. Theoretical investigation of near-field optical properties of tapered fiber tips and single molecule fluorescence. *J Appl Phys* **81**(8):3369–3376.
47. Soper SA, Nutter HL, Keller RA, Davis LM, Shera EB. 1993. The photophysical constants of several fluorescent dyes pertaining to ultrasensitive fluorescence spectroscopy. *Photochem Photobiol* **57**(6):972–977.
48. Eggeling C, Widengren J, Rigler R, Seidel CAM. 1999. Photostability of fluorescent dyes for single-molecule spectroscopy: mechanisms and experimental methods for estimating photobleaching in aqueous solution. In *Applied fluorescence in chemistry, biology and medicine*, pp. 193–240. Ed W Rettig, B Strehmel, S Schrader, H Seifert. Springer-Verlag, New York.
49. Eggeling C, Widengren J, Rigler R, Seidel CAM. 1998. Photobleaching of fluorescent dyes under conditions used for single-molecule detection: evidence of two-step photolysis. *Anal Chem* **70**:2651–2659.
50. Peterman EJG, Brasselet S, Moerner WE. 1999. The fluorescence dynamics of single molecules of green fluorescent protein. *J Phys Chem A* **103**:10553–10560.
51. English DS, Furube A, Barbara PF. 2000. Single-molecule spectroscopy in oxygen-depleted polymer films. *Chem Phys Lett* **324**: 15–19.
52. Deschenes LA, Vanden Bout DA. 2002. Single molecule photobleaching: increasing photon yield and survival time through suppression of two-step photolysis. *Chem Phys Lett* **365**:387–395.

53. Hubner CG, Renn A, Renge I, Wild UP. 2001. Direct observation of the triplet lifetime quenching of single dye molecules by molecular oxygen. *J Chem Phys* **115**(21):9619–9622.
54. Tokunaga M, Kitamura K, Saito K, Iwane AH, Yanagida T. 1997. Single molecule imaging of fluorophores and enzymatic reactions achieved by objective-type total internal reflection fluorescence microscopy. *Biochem Biophys Res Commun* **235**:47–53.
55. Taguchi H, Ueno T, Tadakuma H, Yoshida M, Funatsu T. 2001. Single-molecule observation of protein-protein interactions in the chaperonin system. *Nature Biotechnol* **19**:861–865.
56. Zhuang X, Bartley LE, Babcock HP, Russell R, Ha T, Herschlag D, Chu S. 2000. A single-molecule study of RNA catalysis and folding. *Science* **288**:2048–2051.
57. Ha T, Laurence TA, Chemla DS, Weiss S. 1999. Polarization spectroscopy of single fluorescent molecules. *J Phys Chem B* **103**: 6839–6850.
58. Weiss S. 2000. Measuring conformational dynamics of biomolecules by single molecule fluorescence spectroscopy. *Nature Struct Biol* **7**(9):724–729.
59. Ha T, Glass J, Enderle TH, Chemla DS, Weiss S. 1998. Hindered rotational diffusion and rotational jumps of single molecules. *Phys Rev Lett* **80**(10):2093–2096.
60. Gensch T, Hofkens J, Kohn F, Vosch T, Herrmann A, Mullen K, De Schryver FC. 2001. Polarization sensitive single molecule fluorescence detection with linear polarized excitation light and modulated polarization direction applied to multichromophoric entities. *Single Mol* **2**(1):35–44.
61. Axelrod D. 1989. Fluorescence polarization microscopy. *Methods Cell Biol* **30**:333–352.
62. Bennet JM, Bennet HE. 1978. Polarization, In *Handbook of optics*, pp. 10-1–10-164. Ed WG Driscoll. McGraw-Hill, New York.
63. Forkey JN, Quinlan ME, Goldman YE. 2000. Protein structural dynamics by single-molecule fluorescence polarization. *Prog Biophys Mol Biol* **74**:1–35.
64. Deschenes LA, Venden Bout DA. 2001. Single-molecule studies of heterogeneous dynamics in polymer melts near the glass transition. *Science* **292**:255–258.
65. Deschenes LA, Venden Bout DA. 2001. Molecular motions in polymer films near the glass transition: a single molecule study of rotational dynamics. *J Phys Chem B* **105**:11978–11985.
66. Garcia-Parajo MF, Veerman JA, Segers-Nolten GMJ, de Grooth BG, Greve J, van Hulst NF. 1999. Visualizing individual green fluorescent proteins with a near field optical microscope. *Cytometry* **36**:239–246.
67. Betzig E, Chichester RJ. 1993. Single molecules observed by near-field scanning optical microscopy. *Science* **262**(5138):1422–1425.
68. van Hulst NF, Veerman J-A, Garcia-Parajo MF, Kuipers L. 2000. Analysis of individual (macro)molecules and proteins using near-field optics. *J Chem Phys* **112**(18):7799–7810.
69. Veerman JA, Garcia-Parajo MF, Kuipers L, van Hulst NF. 1999. Single molecule mapping of the optical field distribution of probes for near-field microscopy. *J Microsc* **194**(part 2/3):477–482.
70. Bartko AP, Dickson RM. 1999. Imaging three-dimensional single molecule orientations. *J Phys Chem B* **103**:11237–11241.
71. Dickson RM, Norris DJ, Moerner WE. 1998. Simultaneous imaging of individual molecules aligned both parallel and perpendicular to the optic axis. *Phys Rev Lett* **81**(24):5322–5325.
72. Bohmer M, Enderlein J. 2003. Orientation imaging of single molecules by wide-field epifluorescence microscopy. *J Opt Soc Am B* **20**(3):554–559.
73. Bartko AP, Dickson RM. 1999. Three-dimensional orientations of polymer-bound single molecules. *J Phys Chem B* **103**(16):3053–3056.
74. Bartko AP, Peyser LA, Dickson RM, Mehta A, Thundat T, Bhargava R, Barnes MD. 2002. Observation of dipolar emission patterns from isolated Eu^{3+}:Y_2O_3 doped nanocrystals: new evidence from single ion luminescence. *Chem Phys Lett* **358**:459–465.
75. Tinnefeld P, Herten D-P, Sauer M. 2001. Photophysical dynamics of single molecules studied by spectrally-resolved fluorescence lifetime imaging microscopy (SFLIM). *J Phys Chem A* **105**:7989–8003.
76. Trautman JK, Macklin JJ. 1996. Time-resolved spectroscopy of single molecules using near-field and far-field optics. *Chem Phys* **205**: 221–229.
77. Bohmer M, Pampaloni F, Wahl M, Rahn H-J, Erdmann R, Enderlein J. 2001. Time-resolved confocal scanning device for ultrasensitive fluorescence detection. *Rev Sci Instrum* **72**(11):4145–4152.
78. Heilemann M, Herten DP, Heintzmann R, Cremer C, Muller C, Tinnefeld P, Weston KD, Wolfrum J, Sauer M. 2002. High-resolution colocalization of single dye molecules by fluorescence lifetime imaging microscopy. *Anal Chem* **74**:3511–3517.
79. Lu P, Xun L, Xie XS. 1998. Single-molecule enzymatic dynamics. *Science* **282**:1877–1882.
80. Shi J, Palfey BA, Dertouzos J, Jensen KF, Gafni A, Steel D. 2004. Multiple states of the Tyr318Leu mutant of dihydroorotate dehydrogenase revealed by single-molecule kinetics. *J Am Chem Soc* **126**: 6914–6922.
81. Piestert O, Barsch H, Buschmann V, Heinlein T, Knemeyer J-P, Weston KD, Sauer M. 2003. A single-molecule sensitive DNA hairpin system based on intramolecular electron transfer. *Nanotechnol Lett* **3**(7):979–982.
82. Chruchill MEA. 2003. Watching flipping junctions. *Nature Struct Biol* **10**(2):73–75.
83. McKinney SE Declais A–C, Lilley DMJ, Ha T. 2003. Structural dynamics of individual Holliday junctions. *Nature Struct Biol* **10**(2): 9397.
84. Tan E, Wilson TJ, Nahas MK, Clegg RM, Lilley DMJ, Ha T 2003 A four-way junction accelerates hairpin ribozyme folding via a discrete intermediate. *Proc Natl Acad Sci USA* **100**(16):9308–9313.
85. Zhuang X, Kim H, Pereira MJB, Babcock HP, Walter NG, Chu S. 2002. Correlating structural dynamics and function in single ribozyme molecules. *Science* **296**:1473–1476.
86. Ha T, Zhuang X, Kim HD, Orr JW, Williamson JR, Chu S. 1999. Ligand-induced conformational changes observed in single RNA molecules. *Proc Natl Acad Sci USA* **96**:9077–9082.
87. Kim HD, Nienhaus GU, Ha T, Orr JW, Williamson JR, Chu S. 2002. Mg^{2+}-dependent conformational change of RNA studied by fluorescence correlation and FRET on immobilized single molecules. *Proc Natl Acad Sci USA* **99**(7):4284–4289.
88. Ha T. 2004. Structural dynamics and processing of nucleic acids revealed by single-molecule spectroscopy. *Biochemistry* **43**(14): 4056–4063.
89. Brasselet S, Peterman EJG, Miyawaki A, Moerner WE. 2000. Single-molecule fluorescence resonant energy transfer in calcium concentration dependent cameleon. *J Phys Chem B* **104**:3676–3682.

90. Miyawaki A, Llopis J, Heim R, McCaffery JM, Adams JA, Ikura M, Tsien RY. 1997. Fluorescent indicators for Ca^{2+} based on green fluorescent proteins and calmodulin. *Nature* **388**:882–887.
91. Yildiz A, Tomishige M, Vale RD, Selvin PR. 2004. Kinesin walks hand-over-hand. *Science* **303**:676–678.
92. Yildiz A, Forkey JN, McKinney SA, Ha T, Goldman YE, Selvin PR. 2003. Myosin V walks hand-over-hand: single fluorophore imaging with 1.5-nm localization. *Science* **300**:2061–2065.
93. Kitamura K, Tokunaga M, Iwane AH, Yanagida T. 1999. A single myosin head moves along an actin filament with regular steps of 5.3 nanometers. *Nature* **397**:129–134.
94. Ishii Y, Iwane AH, Yokota HY, Inoue Y, Wazawa T, Nishiyama M, Tanaka H, Kitamura K, Yanagida T. 2002. Studying molecular motors on the single molecule level. In *Single molecule detection in solution: methods and applications*, pp. 273–292. Ed Ch Zander, J Enderlein, RA Keller. Wiley-VCH, Darmstadt, Germany.
95. Sase E, Miyata H, Corrie JET, Craik JS, Kinosita Jr, K. 1995. Real time imaging of single fluorophores on moving actin with an epifluorescence microscope. *Biophys J* **69**:323–328.
96. Ha T, Enderle Th, Chemla DS, Selvin P, Weiss S. 1996. Single molecule dynamics studied by polarization modulation. *Phys Rev Lett* **77**(19):3979–3982.
97. Ha T, Glass J, Enderle Th, Chemla DS, Weiss S. 1998. Hindered rotational diffusion and rotational jumps of single molecules. *Phys Rev Lett* **80**(10):2093–2096
98. Bevington PR, Robinson DK. 1992. *Data reduction and error analysis for the physical sciences*, 2nd ed. McGraw-Hill, New York.
99. Enderlein J, Sauer M. 2001. Optimal algorithm for single-molecule identification with time-correlated single-photon counting. *J Phys Chem A* **105**:48–53.
100. Tellinghuisen J, Wilkerson Jr CW. 1993. Bias and precision in the estimation of exponential decay parameters from sparse data. *Anal Chem* **65**:1240–1246.

ADDITIONAL REFERENCES ON SINGLE-MOLECULE DETECTION

Analytical Chemistry and Single Molecules

Dörre K, Stephan J, Lapczyna M, Stuke M, Dunkel H, Eigen M. 2001. Highly efficient single molecule detection in microstructures. *J Biotechnol* **86**:225–236.

Enderlein J. 1999. Single molecule fluorescence in ultrathin capillaries: an electrodynamic study. *Chem Phys Lett* **301**:430–434.

Fisher BR, Eisler HJ, Stott NE, Bawendi MG. 2004. Emission intensity dependence and single-exponential behavior in single colloidal quantum dot fluorescence lifetimes. *J Phys Chem B* **108**:143–148.

Hanley DC, Harris JM. 2001. Quantitative dosing of surfaces with fluorescent molecules: characterization of fractional monolayer coverages by counting single molecules. *Anal Chem* **73**:5030–5037.

Kang SH, Yeung ES. 2002. Dynamics of single-protein molecules at a liquid/solid interface: implications in capillary electrophoresis and chromatography. *Anal Chem* **74**:6334–6339.

Ludes MD, Wirth MJ. 2002. Single-molecule resolution and fluorescence imaging of mixed-mode sorption of a dye at the interface of C_{18} and acytonitrile/water. *Anal Chem* **74**:386–393.

Ma Y, Shortreed MR, Yeung ES. 2000. High-throughput single molecule spectroscopy in free solution. *Anal Chem* **72**:4640–4645.

Schutz GJ, Gruber HJ, Schindler H, Schmidt TH. 1997. Fluorophores for single molecule microscopy. *J Luminesc* **72–74**:18–21.

Yeung ES. 2001. High-throughput single molecule screening of DNA proteins. *Chem Rec* **1**:123–139.

Co-Localization of Molecules

Lacoste TD, Michalet X, Pinaud F, Chemla DS, Alivisatos AP, Weiss S. 2000. Ultrahigh-resolution multicolor colocalization of single fluorescent probes. *Proc Natl Acad Sci USA* **97**(17):9461–9466.

Osborne MA, Barnes CL, Balasubramanian S, Klenerman D. 2001. Probing DNA surface attachment and local environment using single molecule spectroscopy. *J Phys Chem B* **105**:3120–3126.

Thompson RE, Larson DR, Webb WW. 2002. Precise nanometer localization analysis for individual fluorescent probes. *Phys J* **82**:2775–2783.

Trabesinger W, Hecht B, Wild UP, Schutz GJ, Schindler H, Schmidt TH. 2001. Statistical analysis of single-molecule colocalization assays. *Anal Chem* **73**:1100–1105.

Data Analysis of Single-Molecule Emission

Novikov E, Hofkens J, Cotlet M, Maus M, De Schryver FC, Boens N. 2001. A new analysis method of single molecule fluorescence using series of photon arrival times: theory and experiment. *Spectrochim Acta, Part A* **57**:2109–2133.

Turton DA, Reid GD, Beddard GS. 2003. Accurate analysis of fluorescence decays from single molecules in photon counting experiments. *Anal Chem* **75**:4182–4187.

Dendrimers and Polymers

Bowden NB, Willets KA, Moerner WE, Waymouth RM. 2002. Synthesis of fluorescently labeled polymers and their use in single-molecule imaging. *Macromolecules* **35**:8122–8125.

Gensch T, Hofkens J, Heirmann A, Tsuda K, Verheijen W, Vosch T, Christ T, Basché T, Müllen K, De Schryver FC. 1999. Fluorescence detection from single dendrimers with multiple chromophores. *Angew Chem, Int Ed* **38**(24):3752–3756.

Gronheid R, Hofkens J, Köhn F, Weil T, Reuther E, Müllen K, De Schryver FC. 2002. Intramolecular Förster energy transfer in a dendritic system at the single molecule level. *J Am Chem Soc* **124**(11):2418–2419.

Diffusion or Tracking of Single Molecules

Cao J. 2001. Single molecule tracking of heterogeneous diffusion. *Phys Rev E* **63**:041101-1–041101-7.

Ghosh RN, Webb WW. 1994. Automated detection and tracking of individual and clustered cell surface low density lipoprotein receptor molecules. *Biophys J* **66**:1301–1318.

Hashimoto F, Tsukahara S, Watarai H. 2003. Lateral diffusion dynamics for single molecules of fluorescent cyanine dye at the free and surfactant-modified dodecane–water interface. *Langmuir* **19**:4197–4204.

Ke PC, Naumann CA. 2001. Single molecule fluorescence imaging of phospholipid monolayers at the air–water interface. *Langmuir* **17**: 3727–3733.

Schmidt TH, Schutz GJ, Baumgartner W, Gruber HJ, Schindler H. 1996. Imaging of single molecule diffusion. *Proc Natl Acad Sci USA* **93**: 2926–2929.

Simpson R, Sheets ED, Jacobson K. 1995. Detection of temporary lateral confinement of membrane proteins using single-particle tracking analysis. *Biophys J* **69**:989–993.

Swinton DJ, Wirth MJ. 2001. Single molecule study of the lateral transport of four homooligoncleotides at the interface of water and chemically modified silica. *J Phys Chem B* **105**:8679–8684.

Swinton DJ, Wirth MJ. 2001. Single-molecule study of an adsorbed oligonucleotide undergoing both lateral diffusion and strong adsorption. *J Phys Chem B* **105**:1472–1477.

Tadakuma H, Yamaguchi J, Ishihama Y, Funatsu T. 2001. Imaging of single fluorescent molecules using video-rate confocal microscopy. *Biochem Biophys Res Commun* **287**:323–327.

Xu XH, Yeung ES. 1997. Direct measurement of single-molecule diffusion and photodecomposition in free solution. *Science* **275**:1106–1109.

Xu XH, Yeung ES. 1998. Long-range electrostatic trapping of single-protein molecules at a liquid–solid interface. *Science* **281**:1650–1653.

DNA Applications Using SMD

Anazawa T, Matsunaga H, Yeung ES. 2002. Electrophoretic quantitation of nucleic acids without amplification by single-molecule imaging. *Anal Chem* **74**:5033–5038.

Deniz AA, Dahan M, Grunwell JR, Ha T, Faulhaber AE, Chemla DS, Weiss S, Schultz PG. 1999. Single-pair fluorescence resonance energy transfer on freely diffusing molecules: observation of Förster distance dependence and subpopulations. *Proc Natl Acad Sci USA* **96**: 3670–3675.

Edman L, Mets Ü, Rigler R. 1996. Conformational transitions monitored for single molecules in solution. *Proc Natl Acad Sci USA* **93**: 6710–6715.

Eggeling C, Fries JR, Brand L, Günther R, Seidel CAM. 1998. Monitoring conformational dynamics of a single molecule by selective fluorescence spectroscopy. *Proc Natl Acad Sci USA* **95**:1556–1561.

Gueroui Z, Freyssingeas E, Place B, Berge B. 2003. Transverse fluctuation analysis of single extended DNA molecules. *Eur Phys J E* **11**: 105–108.

Gueroui Z, Place E, Freyssingeas E, Berge B. 2002. Observation by fluorescence microscopy of transcription on single combed DNA. *Proc Natl Acad Sci USA* **99**(9):6005–6010.

Ha T, 2001. Single-molecule fluorescence methods for the study of nucleic acids. *Curr Opin Struct Biol* **11**:287–292.

Ha T, Rasnik I, Cheng W, Babcock HP, Gauss GH, Lohman TM, Chu S. 2002. Initiation and re-initiation of DNA unwinding by the *Escherichia coli* rep helicase. *Nature* **419**:638–641.

Harada Y, Funatsu T, Murakami K, Nonoyama Y, Ishihama A, Yanagida T. 1999. Single-molecule imaging of RNA polymerase–DNA interactions in real time. *Biophys J* **76**:709–715.

Herrick J, Bensimon A. 1999. Imaging of single DNA molecule: Applications to high-resolution genomic studies. *Chromosome Res* **7**:409–423.

Hirose T, Ohtani T, Muramatsu H, Tanaka A. 2002. Direct visualization of abasic sites on a single DNA molecule using fluorescence microscopy. *Photochem Photobiol* **76**(2):123–126.

Kang SO, Shortreed MR, Yeung ES. 2001. Real-time dynamics of single-DNA molecules undergoing adsorption and desorption at liquid–solid interfaces. *Anal Chem* **73**:1091–1099.

Knemeyer JP, Marme N, Sauer M. 2000. Probes for detection of specific DNA sequences at the single-molecule level. *Anal Chem* **72**: 3717–3724.

Osborne MA, Furey WS, Klenerman D, Balasubramanian S. 2000. Single-molecule analysis of DNA immobilized on microspheres. *Anal Chem* **72**:3678–3681.

Schäfer B, Gemeinhardt H, Uhl V, Greulich KO. 2000. Single molecule DNA restriction analysis in the light microscope. *Single Mol* **1**:33–40.

Tachi-iri Y, Ishikawa M, Hirano K. 2000. Investigation of the hydrolysis of single DNA molecules using fluorescence video microscopy. *Anal Chem* **72**:1649–1656.

Werner JH, Cai H, Jett JH, Reha-Krantz L, Keller RA, Goodwin PM. 2003. Progress towards single-molecule DNA sequencing: a one color demonstration. *J Biotechnol* **102**:1–14.

General Papers on SMD

Bloess A, Durand Y, Matsushita M, Van Dermeer HV, Brakenhoff GJ, Schmidt J. 2002. Optical far-field microscopy of single molecules with 3.4 nm lateral resolution. *J Microsc* **205**(1):76–85.

Harbron EJ, Barbara PF. 2002. The Poisson distribution and single-molecule spectroscopy. *J Chem Educ* **79**(2):211–213.

Nie S, Chiu DT, Zare RN. 1994. Probing individual molecules with confocal fluorescence microscopy. *Science* **226**:1018–1021.

Green Fluorescent Protein and Its Mutants

Bowen B, Woodbury N. 2003. Single-molecule fluorescence lifetime and anisotropy measurements of the red fluorescent protein, DsRed, in solution. *Photochem Photobiol* **77**(4):362–369.

Cotlet M, Hofkens J, Habuchi S, Dirix G, Van Guyse M, Michiels J, Vanderleyden J, De Schryver FC. 2001. Identification of different emitting species in the red fluorescent protein DsRed by means of ensemble and single-molecule spectroscopy. *Proc Natl Acad Sci USA* **98**(25):14398–14403.

Dickson RM, Cubitt AB, Tsien RY, Moerner WE. 1997. On/off blinking and switching behaviour of single molecules of green fluorescent protein. *Nature* **388**(6640):355–358.

Garcia-Parajo MF, Koopman M, van Dijk EMHP, Subramaniam V, van Hulst NF. 2001. The nature of fluorescence emission in the red fluorescent protein DsRed, revealed by single-molecule detection. *Proc Natl Acad Sci USA* **98**(25):14392–14397.

Harms GS, Cognet L, Lommerse PHM, Blab GA, Schmidt T. 2001. Autofluorescent proteins in single-molecule research: applications to live cell imaging microscopy. *Biophys J* **80**:2396–2408.

Identification of Single Molecules

Dahan M, Deniz AA, Ha T, Chemla DS, Schultz PG, Weiss S. 1999. Ratiometric measurement and identification of single diffusing molecules. *Chem Phys* **247**:85–106.

Knemeyer J-P, Herten D-P, Sauer M. 2003. Detection and identification of single molecules in living cells using spectrally resolved fluorescence lifetime imaging microscopy. *Anal Chem* **75**:2147–2153.

Intracellular SMD

Byassee TA, Chan WCW, Nie S. 2000. Probing single molecules in single living cells. *Anal Chem* **72**:5606–5611.

Iino R, Koyama I, Kusumi A. 2001. Single molecule imaging of green fluorescent proteins in living cells: e-cadherin forms oligomers on the free cell surface. *Biophys J* **80**:2667–2677.

Iino R, Kusumi A. 2001. Single-fluorophore dynamic imaging in living cells. *J Fluoresc* **11**(3):187–195.

Murakoshi H, Iino R, Kobayashi T, Fujiwara T, Ohshima C, Yoshimura A, Kusumi A. 2004. Single-molecule imaging analysis of Ras activation in living cells. *Proc Natl Acad Sci USA* **101**(19):7317–7322.

Sako Y, Minoguchi S, Yanagida T. 2000. Single-molecule imaging of EGFP signaling on the surface of living cells. *Nat Cell Biol*. **2**:168–172.

Sako Y, Uyemura T. 2002. Total internal reflection fluorescence microscopy for single-molecule imaging in living cells. *Cell Struct Funct* **27**:357–365.

Seisenberger G, Ried MU, Endress T, Buning H, Hallek M, Brauchle C. 2001. Real-time single-molecule imaging of the infection pathway of an adeno-associated virus. *Science* **294**:1929–1932.

van Hulst NF, Garcia-Parajo MF, Moers MHP, Veerman JA, Ruiter AGT. 1997. Near-field fluorescence imaging of genetic material: toward the molecular limit. *J Struct Biol* **119**:222–231.

Low-Temperature Single-Molecule Studies

Moerner WE, Dickson RM, Norris DJ. 1997. Single-molecule spectroscopy and quantum optics in solids. *Adv At, Mol, Opt Phys* **38**:193–236.

Orrit M, Bernard J, Personov RI. 1993. High-resolution spectroscopy of organic molecules in solids: from fluorescence line narrowing and hole burning to single molecule spectroscopy. *J Phys Chem* **97**:10256–10268.

Orrit M, Bernard J. 1990. Single pentacene molecules detected by fluorescence excitation in a *p*-terphenyl crystal. *Phys Rev Lett* **65**(21):2716–2719.

Osad'ko IS. 2003. *Selective spectroscopy of single molecules*. Springer, New York.

Near-Field Scanning Optical Microscopy and Single Molecules

Ambrose WP, Goodwin PM, Martin JC, Keller RA. 1994. Single molecule detection and photochemistry on a surface using near-field optical excitation. *Phys Rev Lett* **72**:(1):160–163.

Azoulay J, Debarre A, Richard A, Tchenio P. 1999. Field enhancement and apertureless near-field optical spectroscopy of single molecules. *J Microsc* **194**(2/3):486–490.

Colas des Francs G, Girard C. 2002. Theory of near-field optical imaging with a single fluorescent molecule used as a point-like detector. *Chem Phys* 2**82**:277–287.

Gimzewski JK, Joachim C. 1999. Nanoscale science of single molecules using local probes. *Science* **283**:1683–1688.

Hamann HF, Gallagher A, Nesbitt DJ. 2000. Near-field fluorescence imaging by localized field enhancement near a sharp probe tip. *Appl Phys Lett* **76**:1953–1955.

Kramer A, Trabesinger W, Hecht B, Wild UP. 2002. Optical near-field enhancement at a metal tip probed by a single fluorophore. *Appl Phys Lett* **80**(9):1652–1654.

Ruiter AGT, Veerman JA, Garcia-Parajo MF, van Hulst NF. 1997. Single molecule rotational and translational diffusion observed by near-field scanning optical microscopy. *J Phys Chem A* **101**:7381–7323.

Sick B, Hect B, Wild UP, Novotny L. 2001. Probing confined fields with single molecules and vice versa. *J Microsc* **202**(2):365–373.

Veerman JA, Levi SA, van Veggel FCJM, Reinhoudt DN, van Hulst NF. 1999. Near-field scanning optical microscopy of single fluorescent dendritic molecules. *J Phys Chem A* **103**:11264–11270.

Xie XS, Dunn RC. 1994. Probing single molecule dynamics. *Science* **265**: 361–364.

Zhang Z, Rajagopalan PTR, Selzer T, Benkovic SJ, Hammes GG. 2004. Single-molecule and transient kinetics investigation of the interaction of dihydrofolate reductase with NADPH and dihydrofolate. *Proc Natl Acad Sci USA* **101**(9):2764–2769.

Photobleaching

Gordon MP, Ha T, Selvin PR. 2004. Single-molecule high-resolution imaging with photobleaching. *Proc Natl Acad Sci USA* **101**(17): 6462–6465.

Ko D-S. 2004. Photobleaching time distribution of a single tetramethylrhodamine molecule in agarose gel. *J Chem Phys* **120**(5):2530–2531.

Tsien RY, Waggoner A. 1995. Fluorophores for confocal microscopy: photophysics and photochemistry. In *Handbook of biological confocal microscopy pawley*, pp. 267–279. Ed JB Pawley. Plenum Press, New York.

van Dijk MA, Kapitein LC, van Mameren J, Schmidt CF, Peterman EJG. 2004. Combining optical trapping and single-molecule fluorescence spectroscopy: enhanced photobleaching of fluorophores. *J Phys Chem B* **108**:6479–6484.

Zondervan R, Kulzer F, Kol'chenko MA, Orrit M. 2004. Photobleaching of rhodamine 6G in (polyvinyl alcohol) at the ensemble and single-molecule levels. *J Phys Chem A* **108**:1657–1665.

Photobleaching of Single Molecules

Basche TH, Kummer S, Brauchle C. 1995. Direct spectroscopic observation of quantum jumps of a single molecule. *Nature* **373**:132–134.

Ha T, Enderle TH, Chemla DS, Selvin PR, Weiss S. 1997. Quantum jumps of single molecules at room temperature. *Chem Phys Lett* **271**:1–5.

Kohn F, Hofkens J, Gronheid R, Van der Auweraer M, De Schryver FCD. 2002. Parameters influencing the on- and off-times in the fluorescence intensity traces of single cyanine dye molecules. *J Phys Chem A* **106**:4808–4814.

Lu HP, Xie XS. 1997. Single-molecule spectral fluctuations at room temperature. *Nature* **385**(6612):143–146.

Wennmalm S, Rigler R. 1999. On death numbers and survival times of single dye molecules. *J Phys Chem* **103**:2516–2519.

Polarization and Orientation of Single Molecules

Bopp MA, Jia Y, Haran G, Morlino EA, Hochstrasser RM. 1998. Single-molecule spectroscopy with 27 fs pulses: time-resolved experiments and direct imaging of orientational distributions. *Appl Phys Lett* **73**(1):7–9.

Güttler F, Croci M, Renn A, Wild UP. 1996. Single molecule polarization spectroscopy: pentacene in p-terphenyl. *Chem Phys* **211**:421–430.

Güttler F, Sepiol J, Plakhotnik T, Mitterdorfer A, Renn A, Wild UP. 1993. Single molecule spectroscopy: fluorescence excitation spectra with polarized light. *J Luminesc* **56**:29–38.

Harms GS, Sonnleitner M, Schutz GJ, Gruber HJ, Schmidt TH. 1999. Single-molecule anisotropy imaging. *Biophys J* **77**:2864–2870.

Hu D, Lu PH. 2003. Single-molecule nanosecond anisotropy dynamics of tethered protein motions. *J Phys Chem B* **107**:618–626.

Kreiter M, Prummer M, Hecht B, Wild UP. 2002. Orientation dependence of fluorescence lifetimes near an interface. *J Chem Phys* **117**(20): 9430–9433.

Lieb MA, Zavislan JM, Novotny L. 2004. Single-molecule orientations determined by direct emission pattern imaging. *J Opt Soc Am B* **21**: 1210–1215.

Sick B, Hecht B, Novotny L. 2000. Orientational imaging of single molecules by annular illumination. *Phys Rev Lett* **85**(21):4482–4485.

Weston K, Goldner LS. 2001. Orientation imaging and reorientation dynamics of single dye molecules. *J Phys Chem B* **105**:3453–3462.

Proteins

Chen Y, Hu D, Vorpagel ER, Lu HP. 2003. Probing single molecule T4 lysozyme conformational dynamics by intramolecular fluorescence energy transfer. *J Phys Chem B* **107**:7947–7956.

Fix M, Melia TJ, Jaiswal JK, Rappoport JZ, You D, Sollner TH, Rothman JE, Simon SM. 2004. Imaging single membrane fusion events mediated by SNARE proteins. *Proc Natl Acad Sci USA* **101**(19):7311–7316

Funatsu T, Harada Y, Tokunaga M, Saito K, Yanagida T. 1995. Imaging of single fluorescent molecules and individual ATP turnovers by single myosin molecules in aqueous solution. *Nature* **374**(6522):555–559.

Ha T, Ting AY, Liang J, Caldwell WB, Deniz AA, Chemla DS, Schultz PG, Weiss S. 1999. Single-molecule fluorescence spectroscopy of enzyme conformational dynamics and cleavage mechanism. *Proc Natl Acad Sci USA* **96**:893–898.

Isshii Y, Yoshida T, Funatsu T, Wazawa T, Yanagida T. 1999. Fluorescence resonance energy transfer between single fluorophores attached to a coiled-coil protein in aqueous solution. *Chem Phys* **247**:163–173.

Margittai M, Widengren J, Schweinberger E, Schroder GF, Felekyan S, Haustein E, Konig M, Fasshauer D, Grubmuller H, Jahn R, Seidel CAM. 2003. Single-molecule fluorescence resonance energy transfer reveals a dynamic equilibrium between closed and open conformations of syntaxin 1. *Proc Natl Acad Sci USA* **100**(26):15516–15521.

Rutkauskas D, Novoderezkhin V, Cogdell RJ, van Grondelle R. 2004. Fluorescence spectral fluctuation of single LH2 complexes from *Rhodopseudomonas acidophila* strain 10050. *Biochemistry* **43**:4431–4438.

Yang H, Luo G, Karnchanaphanurach P, Louie T-M, Rech I, Cova S, Xun L, Xie XS. 2003. Protein conformational dynamics probed by single-molecule electron transfer. *Science* **302**:262–266.

Resonance Energy Transfer in Single Molecules

Allen MW, Bieber Urbauer RJ, Johnson CK. 2004. Single-molecule assays of calmodulin target binding detected with a calmodulin energy-transfer construct. *Anal Chem* **76**:3630–3637.

Deniz AA, Laurence TA, Beligere GS, Dahan M, Martin AB, Chemla DS, Dawson PE, Schultz PG, Weiss S. 2000. Single-molecule protein folding: diffusion fluorescence resonance energy transfer studies of the denaturation of chymotrypsin inhibitor 2. *Proc Natl Acad Sci USA* **97**(10):5179–5184.

Ha T, Ting AY, Liang J, Deniz AA, Chemla DS, Schultz PG, Weiss S. 1999. Temporal fluctuations of fluorescence resonance energy transfer between two dyes conjugated to a single protein. *Chem Phys* **247**: 107–118.

Heilemann M, Tinnefeld P, Mosteiro GS, Parajo MG, Van Hulst NF, Sauer M. 2004. Multistep energy transfer in single molecular photonic wires. *J Am Chem Soc* **126**:6514–6515.

Kapanidis AN, Lee NK, Laurence TA, Doose S, Margeat E, Weiss S. 2004. Fluorescence-aided molecule sorting: analysis of structure and interactions by alternating-laser excitation of single molecules. *Proc Natl Acad Sci USA* **101**(24):8936–8941.

Lee M, Tang J, Hochstrasser RM. 2001. Fluorescence lifetime distribution of single molecules undergoing Förster energy transfer. *Chem Phys Lett* **344**:501–508.

Lipman EA, Schuler B, Bakajin O, Eaton WA. 2003. Single molecule measurement of protein folding kinetics. *Science* **301**:1233–1235.

Rothwell PJ, Berger S, Kensch O, Felekyan S, Antonik M, Wohrl BM, Restle T, Goody RS, Seidel CAM. 2003. Multiparameter single-molecule fluorescence spectroscopy reveals heterogeneity of HIV-1 reverse transcriptase:primer/template complexes. *Proc Natl Acad Sci USA* **100**(4):1655–1660.

Tinnefeld P, Buschmann V, Weston KD, Sauer M. 2003. Direct observation of collective blinking and energy transfer in a bichromophoric system. *J Phys Chem A* **107**(3):323–327.

Yasuda R, Masaike T, Adachi K, Noji H, Itoh H, Kinosita K. 2003. The ATP-waiting conformation of rotating F_1-ATPase revealed by single-pair fluorescence resonance energy transfer. *Proc Natl Acad Sci USA* **100**(16):9314–9318.

Reviews and Monographs on Single-Molecule Detection

Dietrich A, Buschmann V, Müller C, Sauer M. 2002. Fluorescence resonance energy transfer (FRET) and competing processes in donor–acceptor substituted DNA strands: a comparative study of ensemble and single-molecule data. *Rev Mol. Biotechnol* **82**:211–231.

Ishii Y, Yanagida T. 2000. Single molecule detection in life science. *Single Mol* **1**:5–16.

Moerner WE, Basché T. 1993. Optical spectroscopy of single impurity molecules in solids. *Angew Chem, Int Ed* **32**:457–476.

Rigler R, Orrit M, Basche T. 2001. *Single molecule spectroscopy*. Springer, New York.

Xie XS, Trautman JK. 1998. Optical studies of single molecules at room temperature. *Annu Rev Phys Chem* **49**:441–480.

Sensing

Boldt FM, Heinze J, Diez M, Petersen J, Borsch M. 2004. Real-time pH microscopy down to the molecular level by combined scanning electrochemical microscopy/single-molecule fluorescence spectroscopy. *Anal Chem* **76**:3473–3481.

Single-Molecule Detection

Bohmer M, Enderlein J. 2003. Fluorescence spectroscopy of single molecules under ambient conditions: methodology and technology. *ChemPhysChem* **4**:792–808.

Enderlein J. 1999. New approach to fluorescence spectroscopy of individual molecules on surfaces. *Phys Rev Lett* **83**(19):3804–3807.

Spectroscopy of Single Molecules

Basche TH, Moerner WE. 1992. Photon antibunching in the fluorescence of a single dye molecule trapped in a solid. *Phys Rev Lett* **69**(10): 1516–1519.

Deperasinska I, Kozankiewicz B, Biktchantaev I, Sepiol J. 2001. Anomalous fluorescence of terrylene in neon matrix. *J Phys Chem* **105**:810–814.

Donley E, Plakhotnik T. 2001. Luminescence lifetimes of single molecules in disordered media. *J Chem Phys* **114**(22):9993–9997.

Fleury L, Sick B, Zumofen G, Hecht B, Wild UP. 1998. High photo-stability of single molecules in an organic crystal at room temperature observed by scanning confocal optical microscopy. *Mol Phys* **95**(6):1333–1338.

Kador L, Horne DE, Moerner WE. 1990. Optical detection and probing of single dopant molecules of pentacene in a *p*-terphenyl host crystal by means of absorption spectroscopy. *J Phys Chem* **94**:1237–1248.

Kreiter M, Prummer M, Hecht B, Wild UP. 2002. Orientation dependence of fluorescence lifetimes near an interface. *J Chem Phys* **117**(20): 9430–9433.

Hernando J, van der Schaaf M, van Dijk EMHP, Sauer M, Garcia-Parajo MF, van Hulst NF. 2003. Excitonic behavior of rhodamine dimers: a single-molecule study. *J Phys Chem A* **107**:43–52.

Hou Y, Higgins DA. 2002. Single molecule studies of dynamics in polymer thin films and at surfaces: effect of ambient relative humidity. *J Phys Chem B* **106**:10306–10315.

Sanchez EJ, Novotny L, Holtom GR, Xie XS. 1997. Room-temperature fluorescence imaging and spectroscopy of single molecules by two-photon excitation. *Phys Chem A* **101**(38):7019–7023.

Viteri CR, Gilliland JW, Yip WT. 2003. Probing the dynamic guest-host interactions in sol-gel films using single molecule spectroscopy. *J Am Chem Soc* **125**:1980–1987.

Theory of Single-Molecule Fluorescence

Barsegov V, Mukamel S. 2002. Multidimensional spectroscopic probes of single molecule fluctuations. *J Chem Phys* **117**(20):9465–9477.

Berezhkovskii AM, Szabo A, Weiss GH. 1999. Theory of single-molecule fluorescence spectroscopy of two-state systems. *J Chem Phys* **110**(18):9145–9150.

Berezhkovskii AM, Szabo A, Weiss GH. 2000. Theory of fluorescence of single molecules undergoing multistate conformational dynamics. *J Phys Chem B* **104**:3776–3780.

Enderlein J. 2000. Theoretical study of detection of a dipole emitter through an objective with high numerical aperture. *Opt Lett* **25**(9): 634–636.

Enderlein J. 1997. Statistics of single-molecule detection. *J Phys Chem B* **101**:3626–3632.

Schenter GK, Lu HP, Xie XS. 1999. Statistical analyses and theoretical models of single-molecule enzymatic dynamics. *J Phys Chem* **103**: 10477–10488.

Weston KD, Dyck M, Tinnefeld P, Muller C, Herten DP, Sauer M. 2002. Measuring the number of independent emitters in single-molecule fluorescence images and trajectories using coincident photons. *Anal Chem* **74**:5342–5349.

Zheng Y, Brown FLH. 2003. Photon emission from driven single molecules. *J Chem Phys* **119**(22):11814–11828.

Time-Resolved Studies of Single Molecules

De Schryver FC. 1998. Time, space and spectrally resolved photochemistry from ensembles to single molecules. *Pure Appl Chem* **70**(11): 2147–2156.

Fries JR, Brand L, Eggeling C, Kollner M, and Seidel CAM. 1998. Quantitative identification of different single molecules by selective time-resolved confocal fluorescence spectroscopy. *J Phys Chem A* **102**:6601–6613.

Lee M, Kim J, Tang J, Hochstrasser RM. 2002. Fluorescence quenching and lifetime distributions of single molecules on glass surfaces. *Chem Phys Lett* **359**:412–419.

Molski A, Hofkens J, Gensch T, Boens N, De Schryver FC. 2000. Theory of time-resolved single-molecule fluorescence spectroscopy. *Chem Phys Lett* **318**:325–332.

Sauer M, Wolfrum J. 1999. Single-molecule detection in biology with multiplex dyes and pulsed semiconductor lasers. In *Applied Fluorescence in Chemistry, Biology and Medicine*, pp. 39–58. Ed W Rettig, B Strehmel, S Schrader, H Seifert. Springer, New York.

Vallee RAL, Cotlet M, Hofkens J, De Schryver FC. 2003. Spatially heterogeneous dynamics in polymer glasses at room temperature probed by single molecule lifetime fluctuations. *Macromolecules* **36**:7752–7758.

PROBLEMS

P23.1. Suppose you have a fluorophore with a molar extinction of 104,000 M^{-1} cm^{-1} at 600 nm, and a lifetime of 4 ns. Assume there is no intersystem crossing or blinking. Calculate the light intensity in watts/cm^2 needed to result in half of the molecule in the excited state. If the illuminated is 1 μm^2 what is the needed power? Assume the objective transmits 100% of the light.